The Distribution of H2O between Cordierite and Granitic Melt: H2O Incorporation in Cordierite and its Application to High-grade Metamorphism and Crustal Anatexis

Article *in* Journal of Petrology · September 2001

DOI: 10.1093/petrology/42.9.1595

CITATIONS
52

READS
144

2 authors, including:

Simon Leigh Harley
The University of Edinburgh
188 PUBLICATIONS **10,181** CITATIONS

SEE PROFILE

JOURNAL OF PETROLOGY | VOLUME 42 | NUMBER 9 | PAGES 1595–1620 | 2001

The Distribution of H_2O between Cordierite and Granitic Melt: H_2O Incorporation in Cordierite and its Application to High-grade Metamorphism and Crustal Anatexis

S. L. HARLEY* AND D. P. CARRINGTON

DEPARTMENT OF GEOLOGY AND GEOPHYSICS, UNIVERSITY OF EDINBURGH, WEST MAINS ROAD, EDINBURGH EH9 3JW, UK

RECEIVED JUNE 19, 2000; REVISED TYPESCRIPT ACCEPTED FEBRUARY 22, 2001

Experiments defining the distribution of H_2O [D_w = wt % H_2O(melt)/wt % H_2O(crd)]) between granitic melt and coexisting cordierite over a range of melt H_2O contents from saturated (i.e. coexisting cordierite + melt + vapour) to highly undersaturated (cordierite + melt) have been conducted at 3–7 kbar and 800–1000°C. H_2O contents in cordierites and granitic melts were determined using secondary ion mass spectrometry (SIMS). For H_2O vapour-saturated conditions D_w ranges from 4·3 to 7 and increases with rising temperature. When the system is volatile undersaturated D_w decreases to minimum values of 2·6–5·0 at moderate to low cordierite H_2O contents (0·6–1·1 wt %). At very low aH_2O, cordierite contains less than 0·2–0·3 wt % H_2O and D_w increases sharply. The D_w results are consistent with melt H_2O solubility models in which aH_2O is proportional to X_w^2 (where X_w is the mole fraction of H_2O in eight-oxygen unit melt) at $X_w \leq 0{\cdot}5$ and $0{\cdot}25k_w\{exp[(6{\cdot}52 - (2667/T)) \times X_w]\}$ at $X_w > 0{\cdot}5$, coupled with cordierite hydration models in which aH_2O is proportional to $n/(1 - n)$, where n is the number of molecules of H_2O per 18-oxygen anhydrous cordierite formula unit ($n < 1$). Combination of our 800–1000°C cordierite H_2O saturation results with previous cordierite hydration data leads to the following geohydrometer relation, applicable for temperatures in the range 500–1000°C:

$$ln\ K_{eq} = [4203(\pm 320)/T] - 11{\cdot}75\ (\pm 0{\cdot}33)$$

where $K_{eq} = [n_{sat}/(1 - n_{sat})]/fH_2O_{(P,T)}$, n_{sat} is the saturation value of n for the P–T condition of interest, and T is in Kelvin. Moderate to high aH_2O (0·4–0·9) are calculated for H_2O-rich cordierites in several pegmatites and zones of hydrous fluid infiltration in high-grade terrains in Antarctica and central Australia, whereas aH_2O calculated from the measured H_2O contents in cordierites from several granulite migmatites are lower and in the range 0·1–0·4. Calculated H_2O contents of melts that equilibrated with low-H_2O (0·6–1·2 wt %) cordierites in several migmatite terrains are in the range 2·8–4·4 wt %, consistent with dehydration-melting reactions involving biotite (± sillimanite). Calculated melt H_2O contents that in other studied migmatites are unrealistically low for the specified temperature conditions of melting probably reflect post-equilibrium H_2O loss from the cordierites.

KEY WORDS: *cordierite; granite; melting; metamorphism; SIMS*

INTRODUCTION

Fluids and melts interacting with hot rocks during metamorphism and melting at mid- and deep-crustal levels are intrinsic to the evolution of metamorphic belts and the transfer of heat and matter in the crust. As a consequence, it is essential that a thorough understanding of the fluid regime of high-grade metamorphism is developed and constrained using a broad variety of approaches and techniques. The timing and extents of any fluid infiltration, whether by carbonic (CO_2-rich), hydrous or saline fluids (e.g. Newton *et al.*, 1980; Santosh *et al.*, 1990; Shmulovich & Graham, 1996; Buick *et al.*, 1998),

*Corresponding author. Telephone: 0044-131-6508547. Fax: 0044-131-6683184. E-mail: sharley@glg.ed.ac.uk

and prevalence of melt-present but fluid-absent conditions during the course of high-grade metamorphism (e.g. Waters & Whales, 1984; Waters, 1988; Barbey *et al.*, 1990; Stevens & Clemens, 1993) are important factors influencing the behaviour of the deep crust during major tectonic events.

The high temperatures (>800°C) attained in many granulite terrains (Harley, 1989) ensure that some melt has had to be present in equilibrium with solid phases in most metapelitic rocks initially containing biotite, which has been shown experimentally to undergo extensive dehydration melting in the 800–900°C interval for a range of bulk-rock compositions (e.g. Le Breton & Thompson, 1988; Vielzeuf & Holloway, 1988; Puziewicz & Johannes, 1990; Patiño Douce & Johnston, 1991). This general perception is supported by studies of several high-grade terrains in which biotite dehydration-melting reactions have been deduced on the basis of textural (e.g. Vernon & Collins, 1988), petrological (e.g. Waters & Whales, 1984; Bhattacharya & Sen, 1986; Young *et al.*, 1989) and geochemical (e.g. Waters, 1988; Barbey *et al.*, 1990; Holtz & Barbey, 1991) observations from discordant leucosomes and segregations in pelitic gneisses. To understand and quantify the role and influence of melting in granulite generation and probe further into the links between anatexis as manifested in migmatites and felsic magmatism in orogenic belts (Clemens & Vielzeuf, 1987; White & Chappell, 1988; Stevens & Clemens, 1993), it is important to monitor any variations in volatile composition and abundance and deduce accurately the fluid contents of the melts that have migrated within or moved out of the region of high-temperature metamorphism. The melts themselves have crystallized, escaped, fractionated or been affected by post-crystallization metamorphism and so a proxy monitor phase of fluid content is required. This proxy would complement the indirect approaches, such as stable isotopic signatures and mineral equilibria calculations, that are commonly employed to evaluate the extents of fluid interaction and activities of fluid species.

The mineral cordierite, $(Mg,Fe)_2Al_4Si_5O_{18}.(nH_2O, mCO_2)$, potentially provides such a direct mineralogical monitor. Cordierite is able to incorporate both the major volatile species in crustal metamorphism, CO_2 and H_2O, within the channels in its structure and hence can yield information on the relative proportions and contents of those species in any coexisting fluid or melt (Goldman *et al.*, 1977; Armbruster & Bloss, 1980, 1982; Johannes & Schreyer, 1981; Kurepin, 1984; Schreyer, 1985; Le Breton, 1989; Vry *et al.*, 1990). Furthermore, cordierite is a common phase in a variety of metapelitic assemblages and may be produced over a wide pressure (P)–temperature (T) range (3–11 kbar and 600–950°C) through a variety of processes involving rather different fluid regimes, including subsolidus reactions, melting, and metasomatic fluid infiltration. Cordierite-bearing S-type granitoids and upper amphibolite to granulite facies migmatites furthermore indicate that cordierite can occur in equilibrium with peraluminous felsic melts, produced either as a peritectic phase during melting or as a phenocrystic phase during the course of melt crystallization (e.g. Vry *et al.*, 1990; Fitzsimons, 1994, 1996; Harley, 1994; Stevens *et al.*, 1995; Carrington & Harley, 1996).

In fluid-present situations, the absolute abundance of channel volatiles and X_{CO_2} $[CO_2/(CO_2 + H_2O)]$ in cordierite is a function of pressure, temperature and X_{CO_2} in the coexisting fluid (Johannes & Schreyer, 1981; Kurepin, 1984). Hence knowledge of the volatile composition in cordierite provides constraints on the metamorphic fluid composition (e.g. Armbruster & Bloss, 1982; Armbruster *et al.*, 1982; Schreyer, 1985; Vry *et al.*, 1990). However, in cases where a free volatile phase is not present but temperatures are high (>750–800°C: Le Breton & Thompson, 1988; Vielzeuf & Holloway, 1988; Patiño Douce & Johnston, 1991), the absolute abundance of these channel volatiles depends instead upon partitioning of H_2O and CO_2 between the cordierite and a coexisting melt phase of broadly granitic composition (Harley, 1994; Stevens *et al.*, 1995; Carrington & Harley, 1996). Measurements of the total volatile contents and compositions of cordierite formed at known P–T therefore have the potential to discriminate between fluid-present conditions and situations in which melt is present but a free H_2O–CO_2 fluid phase absent and provide quantitative fluid activity estimates to support textural and phase equilibrium approaches. The key prerequisites for this are the availability of (1) reliable and internally consistent experimental data defining the H_2O, and H_2O–CO_2, saturation surfaces for cordierite and (2) related experimental data on the volatile contents of cordierite coexisting with fluid-undersaturated melt (Fig. 1; see Carrington & Harley, 1996) that define the partitioning in the undersaturated system and how this varies with P–T. Of course, application to metamorphic belts also requires spatial data on volatile distribution or zoning in natural cordierite so that the significance of any H_2O or CO_2 leakage from or uptake into the channels in cordierite during post-formation re-equilibration can be assessed (Lepezin & Melenevsky, 1977; Zimmermann, 1981; Jochum *et al.*, 1983; Schreyer, 1985; Mirwald *et al.*, 1986).

This paper presents the results of a polybaric–polythermal experimental study of the partitioning of H_2O between cordierite and coexisting melt that ranges from vapour-saturated to highly undersaturated conditions (Fig. 1), and hence contributes to objectives (1) and (2) in the specific case of the CO_2-free system. Thermodynamic modelling of the experimentally determined H_2O contents of cordierite and melt allows calculation of water activities from cordierite-bearing

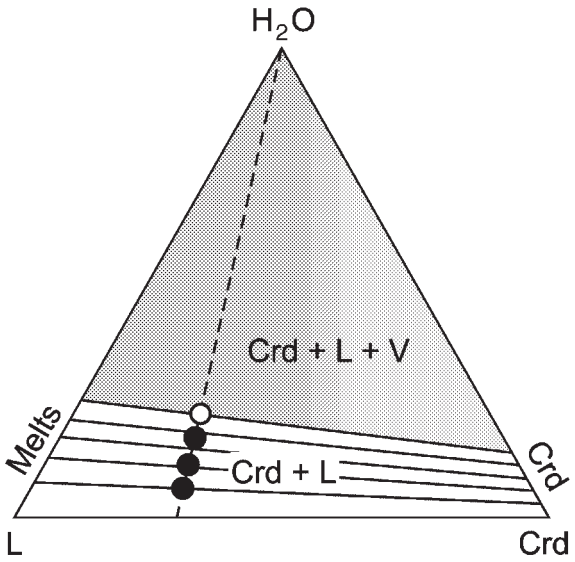

Fig. 1. Schematic composition–assemblage diagram for the system cordierite (Crd)–melt (L)–H_2O at a specific P–T condition, showing the vapour-saturated three-phase field and the bounding Crd–L two-phase field (marked by Crd–L tielines). Four Crd–L experiments are depicted that have similar Crd:L ratios but differ in their bulk H_2O contents and so lie on the schematic line radial to the H_2O apex (dashed line). The experiments access the undersaturated region (e.g. compositions of the lower three filled circles) and also define the saturation condition (compositions at or above the open circle). Tie-lines join Crd and L that coexist for specific $a$$H_2O$ at the given P–T condition.

assemblages and is used to improve present calibrations of the P–T dependence of saturation H_2O contents (isohydrons) in Fe–Mg cordierites. The experimental calibrations are then used to constrain the water activities relevant to high-grade melting and metamorphism both for examples of key mineral reactions constrained from independent experimental data and grids, and for selected granulite and migmatite terrains for which cordierite volatile content data are available.

BACKGROUND AND EXPERIMENTAL RATIONALE

H_2O solubility in felsic and peraluminous melts

The maximum solubilities of H_2O in eutectic melts within the Qz–Ab, Qz–Or, haplogranitic and simplified peraluminous granite systems are now well defined from several studies (e.g. Johannes & Holtz, 1990; Holtz *et al.*, 1992*a*, 1992*b*; Pichavant *et al.*, 1992). Maximum H_2O contents increase strongly with pressure but are only weakly dependent on temperature, and indicate that solubility is also to some extent affected by melt Ab–Or ratio and Al_2O_3 content.

At specified P–T conditions greater than the wet solidus hydrous melts can in principle have H_2O contents anywhere between a maximum that is attained when any additional H_2O forms a free fluid phase (L + V equilibrium: $a$$H_2O$ = 1), and a minimum H_2O content at which the granitic melt crystallizes quartz and alkali-feldspar (L + Crystals equilibrium; Holtz & Johannes, 1994; Johannes & Holtz, 1996); only on the wet and dry solidi are the maximum and minimum H_2O contents identical. This is a key feature of the melt system relevant to the H_2O-undersaturated experiments carried out in this study, which spans both the H_2O-saturated and -undersaturated portions of compositional space defined in the melt–cordierite–H_2O system (Fig. 1). Melt H_2O contents at the minimum boundary are difficult to measure experimentally as melt–crystal mixtures are produced, but are instead calculated using models for the relationships between P, T, $a$$H_2O$ and weight percent H_2O in melts (e.g. Burnham & Nekvasil, 1986; Burnham, 1994; Moore *et al.*, 1995, 1998; Papale, 1997). The H_2O contents of melts formed in dehydration-melting reactions will also lie at a minimum value for the P–T conditions of melting, but hitherto have only been experimentally constrained using modal mass-balance calculations on run products (Vielzeuf & Holloway, 1988; Patiño Douce & Johnston, 1991; Carrington & Harley, 1995). As a consequence, the Burnham & Nekvasil (1986) approach has been widely used in predicting weight percent H_2O in melts formed through dehydration-melting reactions and for estimation of the fertility of metapelitic rocks as sources of granitoid magmas (Clemens & Vielzeuf, 1987; White & Chappell, 1988; Vielzeuf & Clemens, 1992). The mass-balance relations used to predict melt percentages at a given temperature will be affected by the significant and variable H_2O content of cordierite in those cases where it is produced as a peritectic phase coexisting with melt (Stevens *et al.*, 1995; Carrington & Harley, 1996).

H_2O incorporation in cordierite

The maximum volatile contents of cordierite coexisting with H_2O have been experimentally determined for pure Mg-cordierite (Mirwald & Schreyer, 1977; Mirwald *et al.*, 1979; Johannes & Schreyer, 1981), an Mg-rich natural cordierite (Armbruster & Bloss, 1982), and more recently for Fe-cordierite (Boberski & Schreyer, 1990; Mukhopadhyay & Holdaway, 1994). Maximum H_2O occupancies of the channels in cordierite are constrained by structure and have been variously modelled (Newton & Wood, 1979; Lonker, 1981; Martignole & Sisi, 1981; Bhattacharya & Sen, 1985; Carey, 1995) to yield isohydrons of weight percent H_2O (or of molecules of H_2O per 18-oxygen anhydrous formula unit) in cordierite as a function of P–T. Although the models differ in

the calculated positions, slopes and curvatures of the isohydrons it is evident that the maximum H_2O content of cordierite increases strongly with pressure and decreases with temperature. Indeed, the recent models of Carey (1995), Skippen & Gunter (1996) and Holland & Powell (1998) each reproduce most of the available H_2O-system data to within $\pm 0{\cdot}15$ wt % H_2O. These models also demonstrate that the saturation H_2O contents in the T range 500–800°C do not vary with parameters such as X_{Mg} of the cordierite. However, until now, no cordierite H_2O data for T >800°C have been incorporated into the saturation models and, in addition, not all of the available lower-T data have been included in the different analyses. Therefore, in this study we have modelled the saturation H_2O contents of Fe–Mg cordierites over the T range 500–1000°C, using previous literature data and our new experiments, to derive an improved calibration applicable to all metamorphic and igneous cordierites.

EXPERIMENTAL AND ANALYTICAL METHODS

Experimental design and procedures

Experiments aimed at defining the distribution of water between cordierite and melt, D_w [= wt % H_2O(melt)/wt % H_2O(crd)], have been performed at 800, 900 and 1000°C and 3, 5 and 7 kbar in an internally heated gas apparatus at the University of Edinburgh. The experiments have been conducted using the same methods as employed by Carrington & Harley (1996). The pressure and temperature uncertainties associated with the apparatus are $\pm 0{\cdot}2$ kbar and ± 5°C, respectively (Carrington & Harley, 1995). Up to seven charges could be run in one operation at a particular P–T condition and for run times varying between 250 and 400 h.

In most experiments natural Antarctic cordierite (BB3: Brattstrand Bluffs migmatite leucosome; $X_{Mg} = 0{\cdot}64$; sieve fraction 125–250 mm) has been used (Fig. 2a; see Table 2, below), evacuated of all volatiles before the experiment. A more magnesian cordierite (AMNH: American Museum of Natural History specimen, gem fields, Zimbabwe; $X_{Mg} = 0{\cdot}85$), also evacuated, has been used in 7 kbar runs and at equivalent conditions to BB3 to evaluate any effects of cordierite X_{Mg} on H_2O contents. Evacuation of volatiles is accomplished by prolonged stepped heating under high vacuum at temperatures of up to 1200°C, with the sample held for 1 h at each 100°C temperature step below 1200°C, for 2 h at 1200°C, and heated for a minimum of 10 h in total. Secondary ion mass spectrometry (SIMS) analysis of cordierite grain fragments treated using this stepped-heating procedure shows that they are evacuated (i.e. volatile-free) with apparent H_2O and CO_2 contents at or below the SIMS background levels.

The granitic melt has been added in the form of an anhydrous gel ($X_{Mg} = 0{\cdot}25$) synthesized in the K_2O–Na_2O–FeO–MgO–Al_2O_3–SiO_2 system. The compositions of the starting gel and cordierite are given in Tables 1 and 2, respectively. Pre-determined quantities of H_2O have been added to each of the cordierite–gel charges using a microsyringe so that D_w could be measured for a wide range of H_2O contents in the experimental phases. Reversal experiments have been conducted in a similar way, but with the natural BB3 cordierite, which had first been evacuated, re-saturated with pure H_2O at 900°C and 5·0 kbar. This procedure produces a starting cordierite H_2O content of 1·7 wt %, as measured for sampled grain fragments using SIMS. Additional experiments have been carried out using a geometry in which a gel layer is sandwiched between a layer of evacuated-BB3 cordierite and a layer of pre-saturated BB3 cordierite. A series of such 'sandwich' experiments run for durations between 2 h and 2 weeks (Fig. 2b) have been used as part of a time-study to assess the approach to equilibrium in our experiments as a whole.

Following the experiments the charges were punctured and then impregnated with epoxy under vacuum to ensure that the run products retained their spatial and textural integrity. Each charge was then mounted so that the length of the capsule, and hence both cordierite and melt layers, could be exposed by grinding. Most charges contain well-defined cordierite-rich and melt-rich layers, retaining their original geometry (Fig. 2a). A few charges show relative movement of the Crd–L boundary, probably through crystal slumping and convective motion in the melt. Each experiment has been examined using reflected light microscopy and scanning electron microscopy [SEM; secondary electron imagery (SEI) and backscattered electron imagery (BEI)] to monitor the textural relations and features.

Analysis of run products

The H_2O contents of the experimental cordierite and melt have been analysed using SIMS (Tables 3 and 4), and oxides other than H_2O by energy-dispersive SEM and by wavelength-dispersive electron microprobe (EMP) (Tables 1 and 2). An Oxford Instruments scanning electron microscope at the University of Manchester was used, with beam conditions of 1·5 nA and 15 kV, an energy-dispersive spectrometry (EDS)/ZAF-4 analytical correction procedure, and supercooling to −190°C during analysis to minimize loss of alkali counts on the experimental glasses. Analyses obtained using this technique are comparable in terms of the ratios of non-alkali components (i.e. FMAS) with those obtained using EMP on the same samples. The analytical procedure and

Table 1: Mean analyses of selected experimental glasses

Initial gel		MP13B	MP7	MP5	C4-A	C6-1	C16-1	C11-1	C8-4	C14-2
73·30	SiO_2	71·92	72·26	73·80	73·67	74·54	74·35	74·74	72·88	72·66
15·00	Al_2O_3	16·98	16·14	14·98	15·03	14·95	15·89	14·51	15·57	16·53
1·76	FeO	2·05	2·23	1·73	1·84	1·95	1·16	1·72	1·93	2·08
0·34	MgO	1·21	0·93	0·11	0·50	0·67	1·23	0·30	0·53	1·32
4·70	K_2O	3·91	4·19	4·69	4·42	3·91	3·70	4·34	4·51	3·67
4·89	Na_2O	3·93	4·24	4·69	4·55	3·98	3·66	4·38	4·59	3·75
100·00	Total	100·00	100·00	100·00	100·00	100·00	100·00	100·00	100·00	100·00
	H_2O	10·02	7·82	3·38	5·74	9·36	10·40	7·74	5·94	9·18

Totals excluding H_2O are normalized to 100·00 wt % for ease of comparison. Means are averages of 7–10 analyses in each case. Analyses apart from H_2O obtained using the Oxford Instruments scanning electron microscope with EDS (University of Manchester: beam conditions 1·5 nA, 15 kV, −190°C; EDS/ZAF-4 correction) and the Cameca CAMEBAX Microbeam microprobe (University of Edinburgh: beam conditions 20 kV and 10 nA; on-line PAP correction). H_2O contents are averages of 8–10 SIMS analyses of glasses in each experiment (see Table 4).

Table 2: Mean analyses of selected cordierite from the experiments

BB3		MP13B	MP7	MP5	C4-A	C6-1	C6-3	C5-3	C11-3	C14-2
	Cores									
48·12	SiO_2	48·24	47·50	47·98	47·32	47·62	47·00	47·96	48·38	47·49
33·02	Al_2O_3	33·05	32·47	32·87	32·07	33·07	31·99	32·62	32·68	32·14
8·61	FeO	8·39	8·76	8·57	8·71	8·47	8·66	8·42	8·48	8·49
8·57	MgO	8·34	8·24	8·19	8·45	8·23	8·11	8·27	8·20	8·03
0·03	K_2O	0·04	0·07	0·12	0·07	0·02	0·06	0·13	0·07	0·09
0·05	Na_2O	0·12	0·13	0·12	0·12	0·12	0·14	0·09	0·10	0·09
98·42	Total	98·20	97·17	97·87	96·74	97·53	95·97	97·49	97·93	96·23
0·64	X_{Mg}	0·64	0·63	0·63	0·63	0·63	0·63	0·64	0·63	0·63
	Rims									
	SiO_2	48·85	48·64	48·00	48·02	48·71	46·86	47·97	47·99	49·08
	Al_2O_3	33·50	32·86	32·88	32·04	32·59	32·12	32·45	31·67	32·73
	FeO	5·89	5·54	8·49	7·40	5·15	8·59	5·74	11·38	4·10
	MgO	10·07	10·24	8·18	9·26	10·32	7·98	9·93	6·28	10·74
	K_2O	0·10	0·14	0·11	0·12	0·17	0·07	0·19	0·13	0·06
	Na_2O	0·23	0·23	0·12	0·20	0·34	0·14	0·12	0·22	0·27
	Total	98·64	97·67	97·81	97·04	97·29	95·78	96·40	97·68	96·98
	X_{Mg}	0·75	0·77	0·63	0·69	0·78	0·62	0·76	0·50	0·82
	H_2O	1·70	1·54	0·77	1·29	1·79	1·11	0·88	0·87	1·91

Data are given for the core and rims (within 10 mm of edge) of the crystals. Analyses apart from H_2O obtained using the Cameca CAMEBAX Microbeam microprobe (University of Edinburgh: beam conditions 20 kV and 10 nA; on-line PAP correction). H_2O contents are averages of 8–10 SIMS analyses of cordierites in each experiment (see Table 4).

conditions for the SIMS and EMP analysis are as detailed by Carrington & Harley (1996).

SIMS calibration curves have been obtained in each analytical session using H_2O-bearing glasses of appropriate granitic composition and differing but well-known H_2O contents (2·1, 3·9 and 5·6 wt %) and natural cordierite standards with 1·56 ± 0·08 wt % and 0·80 ± 0·06 wt % H_2O. An O^- primary beam at 8 nA

Table 3: H_2O contents (wt %) of experimental cordierites and glasses, 5·0 kbar, 900°C time-study

Experiment	Run time (h)	A-cordierite wt % H_2O (error)	Glass wt % H_2O (error)	H-cordierite wt % H_2O (error)	D_w^{A-Crd} (calculated using A-cordierite)	D_w^{H-Crd} (calculated using H-cordierite)
C12-1	2·5	0·44 (0·05)	1·43 (0·22)	0·79 (0·03)	3·22 (0·60)	1·80 (0·28)
C12-2	7·3	0·74 (0·03)	2·69 (0·20)	0·85 (0·04)	3·65 (0·31)	3·15 (0·28)
C12-3	24·0	0·97 (0·06)	3·73 (0·14)	0·97 (0·04)	3·85 (0·28)	3·84 (0·22)
C12-4	72·2	1·04 (0·04)	4·33 (0·17)	1·04 (0·03)	4·17 (0·22)	4·17 (0·22)
C4-1	240·0	1·11 (0·03)	4·89 (0·07)		4·39 (0·14)	
C4-C	240·0		3·92 (0·09)	0·85 (0·05)		4·60 (0·28)

A-cordierite (A-Crd) contained no volatiles before the experiment (pre-evacuated). H-cordierite (H-Crd) was pre-saturated before the run (1·7 wt % H_2O). Errors as for Table 4.

current was used in all SIMS sessions. Positive secondary ions were measured (H^+, ^{30}Si) with the ion counts determined at an energy offset of 75 V. Each analysis involved 30 cycles of H and Si counts following 5 min burn-in. The mean of the isotope ratios of the last 10 cycles is taken as the final analysis value, and has a statistical counting precision of better than 1% relative. Analyses are expressed as isotopic ratios of $^1H/^{30}Si$ and converted to weight percent H_2O by comparison with standard cordierites or melts. A similar routine has been used in H_2O–CO_2 analysis of natural cordierites and of experimental run products except that SIMS is set up to measure negative secondary ions (H^-, ^{12}C, ^{28}Si). In this case the analyses, expressed as isotopic ratios of $^1H/^{28}Si$ and $^{12}C/^{28}Si$, are converted to weight percent H_2O and CO_2 respectively by comparison with standard cordierites or melts. The standard errors on analytical populations for individual standard melt and cordierite grains are typically $\pm 0{\cdot}2$ and $\pm 0{\cdot}08$ wt % respectively for each analytical session, which yield calibration curves with 2σ uncertainties of 0·15 wt % and 0·06 wt % for melt and cordierite H_2O contents of 3 wt % and 1 wt % respectively. Following SIMS analysis charges were routinely examined under BEI to confirm the positions and textural contexts of each analytical spot (e.g. Fig. 2b–e) and hence establish, for example, whether the melt (glass) analyses had incorporated any fine crystals and cordierite analyses any melt or spinel.

Each experiment has been assessed to determine whether it was conducted at water-saturated or water-undersaturated conditions. The release of fluid on puncturing the capsule and the extensive presence of vesicles in the experimental glasses are interpreted as a sign that the capsule had been water saturated. As described below, the melt water contents in most of these charges matched closely the saturation water contents reported by Holtz & Johannes (1994) and Johannes & Holtz (1996) for melts in closely comparable chemical systems.

EXPERIMENTAL RESULTS

Approach to equilibrium: time-study

A time-study was conducted to assess the convergence towards equilibrium in the experiments. Two separate experimental charges, one with evacuated BB3 cordierite and the other containing pre-saturated BB3 cordierite, were run for 10 days to provide an experimental reversal bracket at an intermediate melt H_2O content of 4–5 wt % (experiments C4-1 and C4-C). These were complemented by four sandwich-style experiments (C12-1 to C12-4) in which evacuated cordierite and re-saturated cordierite layers were separated by a melt layer (Fig. 2b). The sandwich experiment charges each had H_2O added to them individually by microsyringe and so did not have identical initial total H_2O contents. These four experimental charges were then run for different time intervals (Table 3).

The results of the time-study are plotted in Fig. 3. To evaluate the experiments, we have first calculated the value of D_w [= H_2O(melt)/H_2O(cordierite)] using the analysed H_2O contents of the melt and the initially evacuated cordierite at one end of the capsule. This is then compared with the D_w calculated using the analysed H_2O contents of the melt and the initially saturated cordierite at the other end of the capsule. Assessing the experiments in this way largely removes spurious effects of variations in analysed phase H_2O contents, which are due to variations in the amounts of starting materials (including H_2O fluid) added to each experimental charge.

Table 4: H_2O contents of experimental cordierite–glass pairs

Experiment	Cordierite wt % H_2O (error)	Glass wt % H_2O (error)	D_w* (error)
5 kbar, 900°C			
MP13B (saturation)	1·70 (0·05)	10·02 (0·42)	5·91 (0·30)
MP11B	1·69 (0·06)	9·55 (0·14)	5·65 (0·22)
MP7	1·54 (0·05)	7·82 (0·35)	5·09 (0·28)
MP8	1·49 (0·08)	8·09 (0·37)	5·43 (0·37)
C4-B (reversal)	1·38 (0·06)	6·58 (0·24)	4·77 (0·26)
MP6	1·30 (0·05)	5·62 (0·19)	4·34 (0·21)
C4-A (reversal)	1·29 (0·03)	5·74 (0·17)	4·47 (0·17)
DG4	1·28 (0·07)	5·14 (0·28)	4·02 (0·30)
C4-1	1·11 (0·03)	4·89 (0·07)	4·39 (0·14)
C4-C (reversal)	0·85 (0·05)	3·92 (0·09)	4·60 (0·28)
MP5	0·77 (0·05)	3·38 (0·10)	4·38 (0·31)
MP3	0·56 (0·05)	2·03 (0·10)	3·62 (0·38)
MP2	0·45 (0·02)	2·23 (0·13)	4·97 (0·38)
5 kbar, 800°C			
C6-1 (saturation)	1·79 (0·07)	9·36 (0·19)	5·23 (0·24)
C7-2	1·63 (0·09)	8·17 (0·30)	5·02 (0·34)
C6-5 (reversal)	1·54 (0·05)	6·51 (0·18)	4·23 (0·18)
C6-2	1·45 (0·02)	6·92 (0·18)	4·76 (0·14)
C7-3 (reversal)	1·45 (0·07)	5·20 (0·30)	3·59 (0·27)
C7-4	1·41 (0·11)	6·11 (0·07)	4·32 (0·33)
C6-6 (reversal)	1·21 (0·05)	4·41 (0·07)	3·63 (0·17)
C6-3	1·11 (0·03)	4·39 (0·38)	3·94 (0·36)
5 kbar, 1000°C			
C16-1 (saturation)	1·68 (0·07)	10·40 (0·20)†	6·20 (0·28)
C16-2 (low melt?)	1·45 (0·08)	5·43 (0·27)	3·76 (0·28)
C5-3	0·88 (0·04)	4·17 (0·20)	4·73 (0·30)
C5-4	0·36 (0·01)	2·15 (0·10)	5·93 (0·29)
3 kbar, 800°C			
C11-1 (saturation)	1·44 (0·03)	7·74 (0·24)	5·34 (0·21)
C11-4 (reversal)	1·15 (0·03)	5·78 (0·24)	5·04 (0·25)
C11-2	0·98 (0·03)	4·02 (0·17)	4·12 (0·21)
C11-3	0·87 (0·04)	3·25 (0·19)	3·74 (0·28)
3 kbar, 900°C			
C8-4 (reversal)	1·17 (0·05)	5·94 (0·18)	5·08 (0·28)
C8-1	1·11 (0·06)	5·46 (0·22)	4·92 (0·33)
C8-2	0·85 (0·05)	3·68 (0·04)	4·34 (0·24)
C8-5 (reversal)	0·71 (0·04)	3·66 (0·03)	5·13 (0·30)
C8-3	0·51 (0·01)	2·57 (0·12)	5·07 (0·26)
7 kbar, 900°C			
C18-1 (saturation)	2·17 (0·16)	13·25 (0·20)†	6·11 (0·44)
C14-2	1·91 (0·14)	9·18 (0·35)	4·82 (0·41)

*Partition coefficient. $D_w = (H_2O)^{glass}/(H_2O)^{cordierite}$. Error propagated from errors in phases.
†The extreme volatility of these very high water content glasses made SIMS analysis unreliable and the values shown are estimates from data of Holtz & Johannes (1994), with which our other data agree very closely. Saturation experiments are those containing a pure H_2O phase, reversal experiments are those in which the cordierite was pre-saturated with pure H_2O (i.e. experiments using H-Crd).
Errors are 1σ standard deviations propagated from variations in the analysis populations ($n \sim 8$–10) for each phase in each experiment.

The two calculated values of D_w converge to within error after only 24 h and continue to be comparable for up to 240 h run duration, the shortest run duration used for the principal equilibrium experiments of this study. The increase in the D_w calculated using the pre-evacuated cordierite with increasing run duration is opposite to that which would be expected for identical experimental charges with identical total H_2O contents. This trend, and that of overall increase in the converged D_w obtained from 24 h to 240 h, results from the differing total H_2O content of each experiment. As is demonstrated by the full experimental dataset, D_w at a selected P–T condition is generally observed to increase with increasing H_2O contents in the phases (see below). The convergent time-study results are consistent with this, and it is coincidental that the time-study experiments with the lowest total H_2O contents (i.e. bulk weight percent H_2O in the experimental charge) happen to be those with the shorter run durations. We are confident that the value of D_w reached at 240 h is close to equilibrium, as six previous and comparable experiments (Carrington & Harley, 1996) with run durations from 280 to 340 h show an average D_w of 4·4 ($\pm$ 0·6), indistinguishable from the results of this time-study.

Phase chemistry

Glasses (melts)

The melt gel composition (Table 1) has been selected to be close to the eutectic composition and in Fe–Mg equilibrium with BB3 cordierite (Table 2) at the central P–T conditions of the study, 900°C and 5·0 kbar (Carrington & Harley, 1996). The experimental glasses have been analysed to detect any significant deviations from eutectic compositions, which would result in reduced melt water contents at a given P–T condition (Table 2). Analyses have been obtained by analytical SEM using a liquid-nitrogen cold stage to minimize the alkali counting losses that are common in water- and alkali-rich glasses (SEM, Fig. 4), and with a Cameca CAMEBAX electron microprobe (EMP, Fig. 4) to cross-check the accuracy of SiO_2, Al_2O_3, FeO and MgO as measured on the cold-stage scanning electron microscope. EMP analyses show variable to extensive alkali losses, leading to high normative quartz (Fig. 4), but project back into the cluster of analyses obtained by SEM. Hence the reported glass analyses, which show only minor variation in SiO_2, Al_2O_3 and FeO centred around the starting composition, are reliable. The analysed glasses have consistently higher MgO and lower Na_2O and K_2O contents than the initial gel, but their compositional range overlaps that of eutectic compositions measured in independent experimental studies over a range of P–aH_2O conditions (Johannes & Holtz, 1996, fig. 2.20). As the melts produced in our

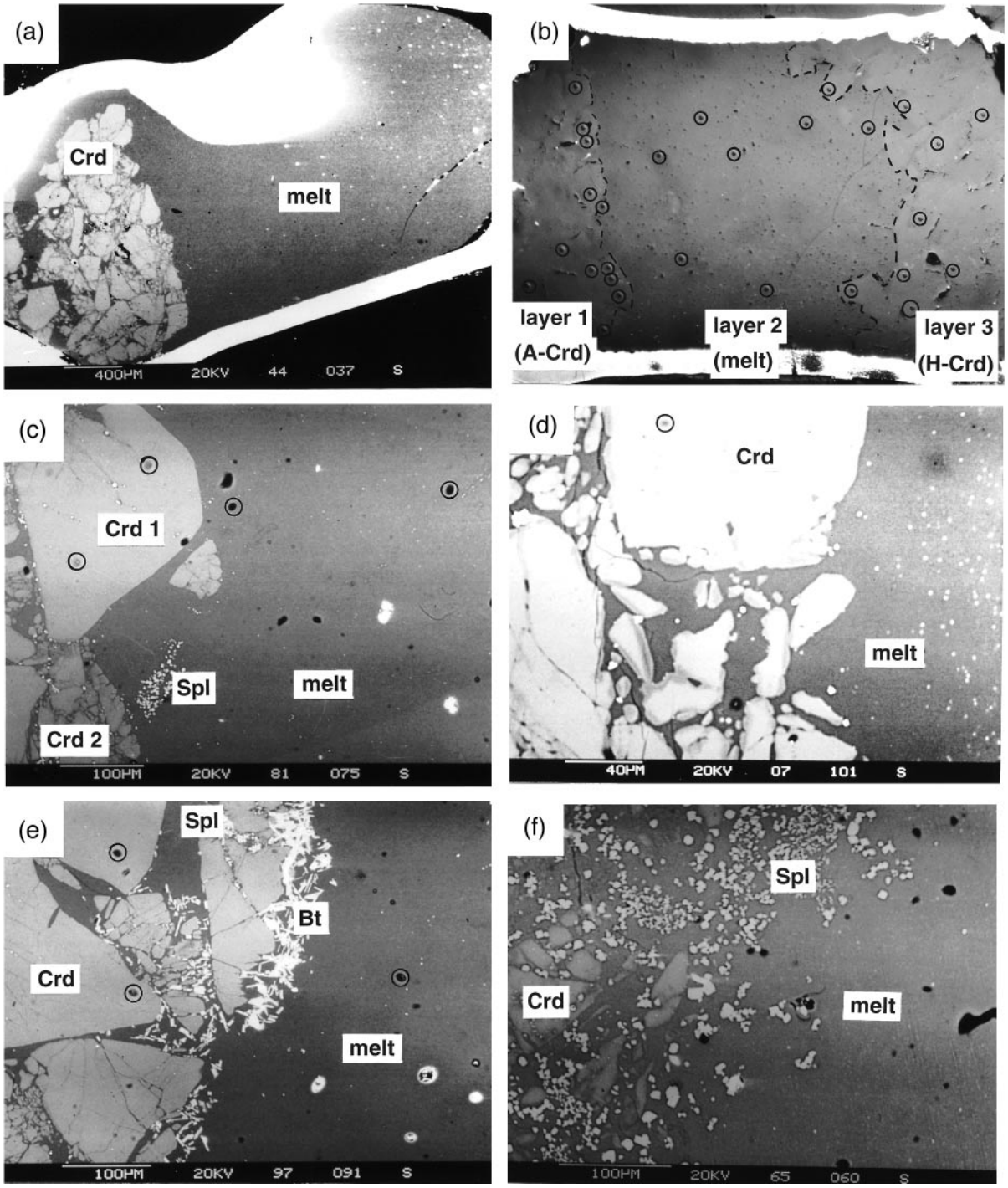

Fig. 2.

experiments appear to be close to eutectic compositions, any decrease in the maximum melt H_2O content attainable at a given P–T condition arising from compositional variation is significantly less than the variations resulting from changes in pressure and aH_2O.

In detail, normative quartz (Fig. 4) increases with increasing weight percent H_2O to contents that are high compared with haplogranitic eutectic melts but consistent with independent experimental results for peraluminous melts character (Johannes & Holtz, 1996). Normative

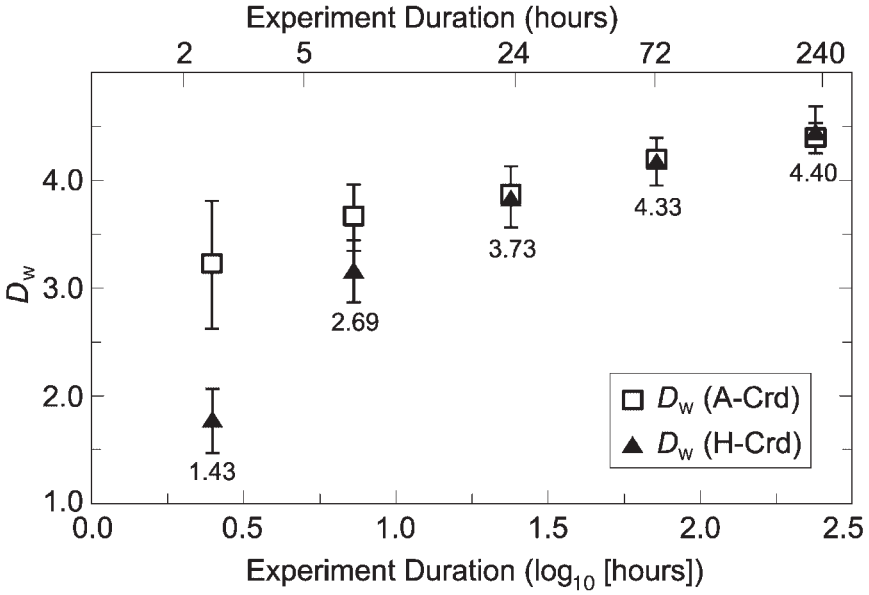

Fig. 3. D_w plotted against experimental run duration for the time-study experiments conducted at 5·0 kbar and 900°C. After 24 h the D_w calculated using the initially H_2O-saturated cordierite (H-Crd) converges with that calculated using the initially evacuated cordierite (A-Crd) data. The trend of increasing D_w with time is an artefact of the differing bulk H_2O contents of the different sandwich experiments, as monitored by the average melt H_2O contents (numbers under each experimental pair, in wt %). (See text for further explanation.)

corundum in the experimental glasses increases from 2·2 to 6·2% in parallel with the increase in normative quartz. The higher levels of normative corundum are greater than that attained in haplogranite experiments (Johannes & Holtz, 1996), although comparable with those of natural leucogranites and rhyolites. The maximum melt H_2O content at fluid saturation is not significantly dependent on normative corundum content, and for the total variation in normative corundum seen in our experimental study there is a variation of only 0·5 wt % in the maximum melt H_2O content attainable at a specified P–T condition (Johannes & Holtz, 1996, fig. 4.8). The more quartz-normative of our experimental glasses are less orthoclase-normative than the previously determined eutectic compositions, but this deviation is unlikely to affect the maximum melt H_2O contents greatly as the Or/Ab ratio has only a small effect on H_2O solubility for the limited range of compositions (Or/Ab = 0·7–0·82) produced in this study (Holtz *et al.*, 1992*a*, 1992*b*).

Cordierite

The cordierite crystals generally retain their original composition with respect to major oxides other than H_2O. There are changes in the Fe/Mg ratio of the crystal rims and increases in the minor alkali content of the cordierites (Table 3).

The melt (X_{Mg} = 0·25) and cordierite (BB3: X_{Mg} = 0·64) compositions were originally chosen to be in Fe/

Fig. 2. (*opposite*) SEM and reflected light images of experimental configurations and run products. It should be noted that in each case 'melt' refers to quenched melt that now is present as a glass. (a) Back-scattered electron (BSE) image of a typical two-layer experiment showing a layer of pre-crushed cordierite fragments (pre-evacuated BB3) and adjacent homogeneous glass formed from melt. Run C6-1, H_2O-saturated, 800°C, 5 kbar. (b) Reflected light image of a three-layer (sandwich) time-study experiment. A layer of pre-crushed and pre-evacuated BB3 cordierite at one end of the capsule (layer 1: A-Crd denotes initially anhydrous cordierite) is separated from pre-crushed but pre-hydrated BB3 cordierite (layer 3: H-Crd denotes pre-hydrated cordierite) at the other end of the capsule by a layer of homogeneous glass formed from quenched melt (layer 2). Run C12-2, H_2O-undersaturated, 900°C, 5 kbar. Elliptical spots (circled) are SIMS analysis pits in each phase; averaged H_2O contents are given in Table 3. (c) BSE image of a cordierite–melt interface region. Circled spots are SIMS analysis pits. [Note clean Crd–L contacts on the large grain (Crd1) and the break-up of another cordierite grain (Crd2) that has a darker BSE appearance because of increased X_{Mg}.] Fine granules of spinel are located along cleavage in Crd1, on grain boundaries and form a cluster in the melt. Run C6-5, H_2O-undersaturated, 800°C, 5 kbar. (d) BSE image of a cordierite–melt interface region. BB3 cordierite fragments show thin rims (2–8 μm in width) with higher X_{Mg} (darker in BSE) than the initial composition. Fine bright grains are spinel, which preferentially occurs in melt in this case. Run C6-1, H_2O-saturated, 800°C, 5 kbar. (e) BSE image of a cordierite–melt interface region. Elliptical spots are SIMS analysis pits (some circled). The cordierite adjacent to melt that is partially replaced by spinel (fine granules) and biotite (elongate grains) has not been used for H_2O content and D_w measurement. Run C6-2, H_2O-undersaturated, 800°C, 5 kbar. (f) BSE image of a cordierite–melt interface region in which initial BB3 cordierite has been extensively resorbed and replaced by spinel (bright equant grains), a feature common in high-H_2O experiments at 3–5 kbar and 1000°C. Run C5-3, H_2O-undersaturated, 1000°C, 5 kbar.

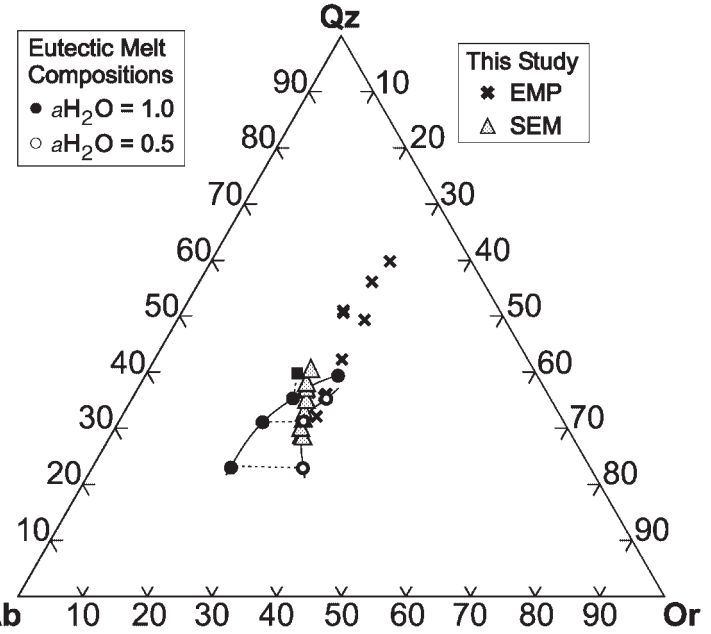

Fig. 4. Normative quartz–albite–orthoclase contents for representative experimental melts, analysed by SEM with a cold stage (Manchester: grey triangles) and by EMP without a cold stage (Edinburgh: ×). Circles represent the eutectic melt compositions for the metaluminous Qz–Ab–Or system at 1, 2, 5 and 10 kilobars, with lower normative Qz at the higher pressures. The filled square is the eutectic composition for a peraluminous melt in the Qz–Ab–Or–Al_2O_3 system at 2 kbar and $aH_2O = 1$. Eutectic data are from Johannes & Holtz (1996; figs 2.20 and 4.3).

Mg equilibrium at 900°C, 5·0 kbar and low aH_2O (Carrington & Harley, 1995, 1996). At other conditions rims of higher, and occasionally lower, cordierite X_{Mg} are observed (Fig. 2d). The rims have a maximum thickness of 10 μm and their X_{Mg} increases with higher-P–T run conditions. In some runs grains of an evacuated cordierite with higher X_{Mg} (AMNH: $X_{Mg} = 0{\cdot}85$) were used, to limit any reaction with melt and provide comparisons with lower-X_{Mg} cordierite. The maximum H_2O content of cordierite attained at any specified P–T condition, in terms of moles per formula unit, has been demonstrated to be independent of its X_{Mg} (Boberski & Schreyer, 1990; Carrington & Harley 1996).

Cordierites show increased Na_2O contents (to 0·32 wt %) that are essentially independent of both T and H_2O content. Cordierite K_2O contents increase with rising T (to 0·19 wt %) and decreasing H_2O, and are in all cases higher than in the starting grains. The lack of correlation between T and Na_2O in the cordierites in our experiments is inconsistent with the Na_2O in cordierite geothermometer devised by Mirwald (1986), but the measured Na contents at 800–900°C and 5 kbar (Crd rims 0·04–0·07 Na cations p.f.u.) are comparable with Na contents reported at similar conditions by Knop *et al.* (1998). The relationships between cordierite alkali contents (both Na and K) and T–aH_2O in our experiments have been described and analysed in detail elsewhere (Thompson *et al.*, 2001) and will not be considered further here as they have no discernible bearing on the H_2O data.

The potential for channel alkalis in cordierite to block the passage of water has been noted in previous diffusion studies (e.g. Johannes & Schreyer, 1981; Zimmermann, 1981). However, for two reasons we suggest that the increased alkali content of the cordierite in our experiments is more likely to prevent water loss on quenching than prevent water entry during the early stages of the run. First, the majority of the starting cordierite grains are initially anhydrous (as confirmed by SIMS analysis of evacuated grains) but end the experiments containing significant water. Second, the measured water contents of the phases in the water-saturated experiments are found to be very close to those found in previous studies conducted on cordierites of varied Fe/Mg ratio and synthesized both with and without alkalis.

In a small number of experiments, a few modal percent of new phases formed. Orthopyroxene was formed very rarely, as fine crystals in the melt. Biotite, feldspar and quartz were occasionally found in melt or on cordierite at the cordierite–melt interface in the lower-temperature runs (Fig. 2e). Spinel was found in the higher-P and -T experiments, usually formed on resorbed cordierite grain boundaries or along fractures in cordierite (Fig. 2b and f). At the highest-T, lowest-P H_2O-rich run conditions (e.g. 1000°C, 3 kbar) cordierite showed extensive resorption and replacement by granular spinel, presumably

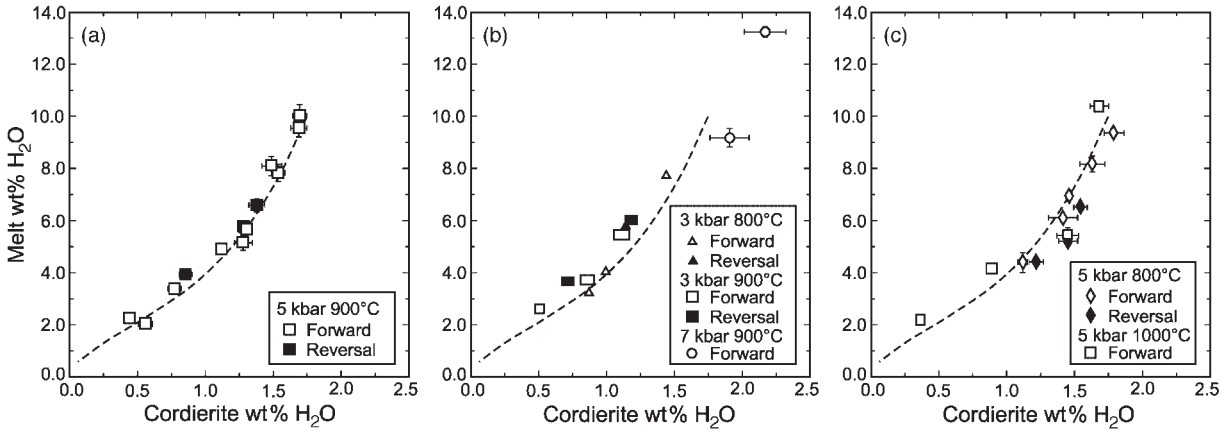

Fig. 5. H_2O contents (wt %) for experimental cordierite–melt (glass) pairs. The curve superimposed on the data at 5·0 kbar, 900°C (a) is calculated from the final modelling of the complete dataset and is not a specific fit to the data shown in (a). The position and curvature of this modelled line depend only on the saturation H_2O contents of cordierite and melt at 5·0 kbar and 900°C and the activity models presented in equations (9), (12a) and (12b) in the text. This modelled curve is reproduced in (b) and (c) for comparative purposes to illustrate the relative displacement of the data with P and T.

as a result of incongruent dissolution in the H_2O-rich melts via the reaction Crd = Spl + $SiO_{2(L)}$ (Fig. 2f). Cordierite–melt H_2O contents measured from such charges have not been used in the data analysis and are not reported here.

Equilibrium H_2O contents in cordierites and glasses (melts)

The H_2O-content results of the experiments are presented in Table 4 and illustrated in three types of diagram to facilitate comparisons of experiments at single P–T conditions and to allow comparisons between polybaric and polythermal data. First, the averaged phase H_2O wt % data are plotted simply as H_2O wt % in melt against H_2O wt % in coexisting cordierite for specified P–T conditions in Fig. 5. Second, the distribution coefficient D_w [= wt % H_2O(melt)/wt % H_2O(Crd)] calculated from such data is plotted against the H_2O content of the product cordierite for given sets of P–T conditions in Fig. 6. Lastly, the normalized H_2O content of melt is plotted against the normalized H_2O of cordierite in Fig. 7. In the last type of diagram the measured H_2O content of each phase is normalized against its maximum H_2O content at fluid saturation at the specified P–T condition. This procedure effectively normalizes isobaric–isothermal data against unit water activity ($a$$H_2O$) and hence allows comparison of all data with the effects of P and T on the maximum H_2O contents attained at $a$$H_2O$ = 1 accounted for.

Melt–cordierite H_2O content data at specified P–T conditions

H_2O content data obtained at 5·0 kbar and 900°C (Fig. 5a) define a smooth and coherent convex trend. The melt H_2O content varies from 10·0 to 2·1 wt %, which by comparison with the data of Holtz & Johannes (1994) spans the entire range from the maximum ($a$$H_2O$ = 1·0) to minimum possible H_2O contents ($a$$H_2O$ ≪ 1·0). Coexisting cordierite H_2O contents vary from 1·70 to ∼0·50 wt %. The curvature of this H_2O distribution trend, previously described as a 'dog-leg' and ascribed to solubility mechanism effects in the melt (Carrington & Harley, 1996), is discussed further in a later section. The forward and reversal experiments are indistinguishable, consistent with a close approach to equilibrium.

The remainder of the data are presented in Fig. 5b and c. The 7·0 kbar, 900°C experiments (Fig. 5b) produced considerably higher maximum (saturation) melt and cordierite H_2O contents than those at 5 kbar, consistent with published data for both phases (Holtz & Johannes, 1994; Mirwald *et al.*, 1979). The 3·0 kbar, 900°C undersaturated experiments have slightly lower cordierite H_2O contents for a given melt H_2O content, when compared with 5·0 kbar data. Also included in Fig. 5b are data from experiments at 3·0 kbar and 800°C, which follow the same trend as that of the 5·0 kbar, 900°C data. All the reversal experiments shown in Fig. 5b are consistent with smooth trends defined by the forward experiments. The isobaric data (Fig. 5c) reproduce the range of melt and cordierite water contents measured at 5·0 kbar and 900°C. The 5·0 kbar, 800°C data show slightly higher cordierite H_2O contents for a given melt H_2O content, whereas three of the four 5·0 kbar, 1000°C data demonstrate lower cordierite H_2O contents for a specified melt H_2O. The one discrepant undersaturated experiment at this P–T condition (C16-2) is attributed to H_2O loss from the quenched melt glass, probably during sample preparation for SIMS. The forward and reversal experiments run at 5·0 kbar, 800°C produce results within

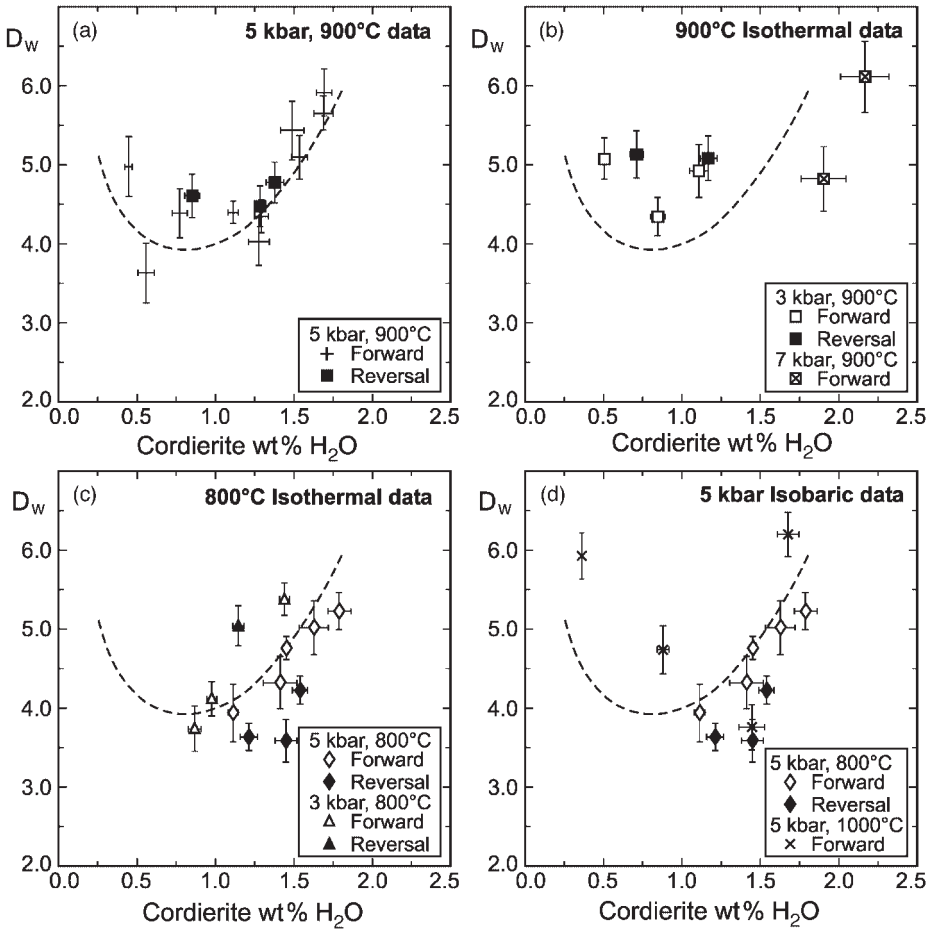

Fig. 6. Variation of the distribution coefficient D_w [= H_2O wt %(melt)/H_2O wt %(Crd)] with H_2O contents of cordierite at specified P–T conditions. (a) Data for 5·0 kbar, 900°C. The expected model D_w trend derived from the saturation H_2O contents of cordierite and melt at this P–T condition (see Fig. 8), reproduced in (b)–(d) for comparisons, is depicted as a dashed curve. At most other P–T conditions the experimental data do not extend to the minimum possible cordierite and melt H_2O contents (from Holtz & Johannes, 1994) attainable. (b) and (c) present isothermal data at 900 and 800°C, respectively; (d) depicts isobaric data at 5 kbar.

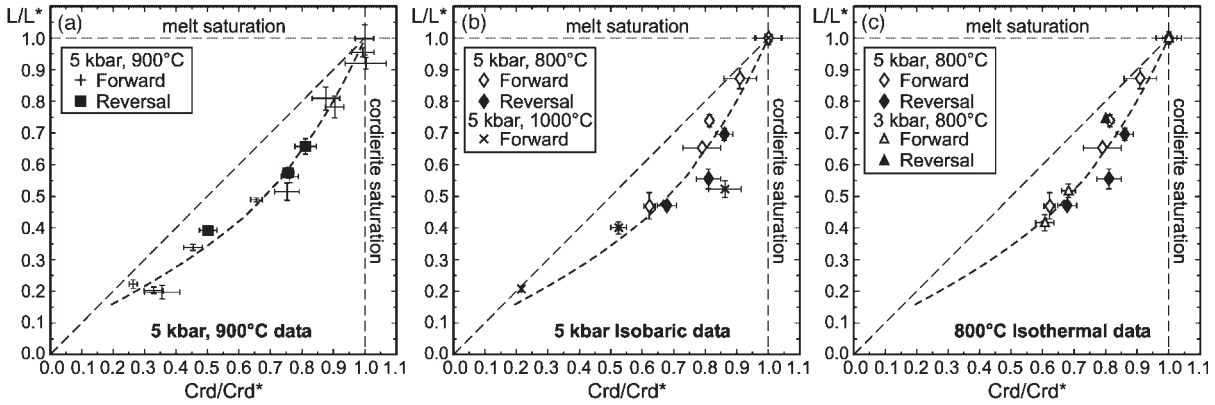

Fig. 7. Normalized diagrams for experimental cordierite–glass (melt) pairs. L/L* is the measured H_2O content of an experimental melt as a proportion of the maximum H_2O content for the melt at the P–T of the experiment. At saturation L/L* = 1·0. Crd/Crd* is the same ratio expressed for cordierite. The dashed curve in (a)–(c) is the predicted normalized H_2O distribution, calculated from the saturation H_2O contents of cordierite and melt at 5·0 kbar and 900°C and the activity models presented in equations (9), (12a) and (12b).

error of each other, although the cordierite water contents are systematically higher for the reversal experiments. A close, but not necessarily complete, approach to equilibrium is therefore inferred for these lower-temperature experiments.

Also depicted in Fig. 5 are reference distribution curves derived from modelling of the entire cordierite–melt dataset, as explained in a later section. These modelled distribution curves bracket all the experimental data but, it should be noted, are not curves fitted to individual datasets collected at specific *P–T* conditions. The curves, derived from the modelling described below, display a convexity that is consistent with the general curvature of the cordierite–melt H_2O data obtained at each *P–T* condition.

D_w–*cordierite* H_2O *content relationships*

The distribution of H_2O between the experimental melt and cordierite pairs is illustrated in Fig. 6. The data obtained at 5·0 kbar and 900°C show that the distribution coefficient, D_w, is 5·9 (± 0·3) for H_2O-saturated conditions and decreases smoothly to 4·2 (± 0·4), before possibly rising again to 5·0 (± 0·4) at the minimum cordierite H_2O content attained. These data straddle and are consistent with a parabolic D_w–H_2O(Crd) curve as depicted in Fig. 6a that has been produced from thermodynamic modelling of the entire dataset (continuous line) and calculated at 5·0 kbar and 900°C; the curve itself is not an explicit fit to the data presented in Fig. 5a.

The data from the experiments conducted at other *P–T* conditions are comparable in form with the results at 5·0 kbar and 900°C but demonstrate systematic *P–T*-dependent effects, in general being displaced consistently upwards (for higher *T*–lower *P*) or downwards (for lower *T*–higher *P*) with respect to the 5·0 kbar and 900°C data and its modelled trend. Isothermal data at 900°C (Fig. 6b) and 800°C (Fig. 6c) indicate that D_w increases with decreasing pressure for a given cordierite H_2O content. The isobaric data at 5·0 kbar (Fig. 6d) and 3·0 kbar (Fig 6e) demonstrate that D_w increases with rising temperature for a given cordierite H_2O content. The highly undersaturated experiment at 5·0 kbar and 1000°C (C5-4) that produced cordierite with a H_2O content of only 0·36 wt % (Fig. 6d) appears to have an anomalously high D_w that is close to that otherwise attained only at saturation for this *P–T* condition. However, the thermodynamic modelling presented in the next section shows that at high temperatures where the minimum H_2O contents of both the melt and cordierite are very low, high values of D_w are to be expected, as illustrated by the convex form of the modelled D_w–H_2O function superimposed on the data for comparative purposes.

Only the data obtained at 5·0 kbar, 900°C and 3·0 kbar, 800°C span the whole range of melt H_2O contents from the maximum to minimum values given by Holtz & Johannes (1994). Our data at the other *P–T* conditions represent partial trends from saturation (or near-saturation) to lower, but not the lowest possible, H_2O contents in coexisting melt and cordierite. This applies in particular to the 7·0 kbar, 900°C dataset (Fig. 6b), which lies parallel to the steeply decreasing part of the D_w trend seen in the 5·0 kbar, 900°C data and the modelled distribution curve. As will be seen in the modelling section, the shapes of the D_w–H_2O (Crd) trends and range of values of D_w for all data except one H_2O-undersaturated saturated Crd–L data point at 5 kbar, 1000°C (Fig. 6d) and a minimum-H_2O data point at 3·0 kbar, 800°C (Fig. 6c) are consistent with simple thermodynamic formulations for the incorporation of H_2O in both melt and cordierite.

Normalized melt–cordierite H_2O *relationships*

Further interpretation of the experimental results from Figs 5 and 6 is complicated by the variations in the maximum H_2O contents of the phases that arise from the different *P–T* conditions used in the experiments. To account for the *P–T*-dependent differences in the maximum H_2O contents, and therefore compare the H_2O-distribution behaviour over the whole *P–T* range of the experimental study, the H_2O contents of both melt and cordierite are expressed as a fraction of the maximum H_2O content in the phase at that *P–T* condition. At 5·0 kbar, 900°C; 5·0 kbar, 800°C; and 3 kbar, 800°C, the maximum fluid contents in cordierite and melt are taken from the experiments reported in this study. Maximum-H_2O melt compositions obtained at 5·0 kbar, 1000°C and 7 kbar, 900°C, however, are considered to be unreliable because of H_2O loss from the quenched glasses, as noted above, and hence in these cases the maximum melt H_2O content at fluid saturation is taken from Holtz & Johannes (1994) and the cordierite from our experiments. As fluid-saturated conditions were not attained at 3 kbar, 900°C, this *P–T* dataset is not presented in Fig. 7. The normalized parameters used for presentation of the data in the polybaric–polythermal diagrams of Fig. 7 are

$$\mathrm{L/L^*} = [\text{wt \% } H_2O \text{ in melt (measured)}]/[\text{wt \% } H_2O \text{ in melt at saturation (L*)}]$$

and

$$\mathrm{Crd/Crd^*} = [\text{wt \% } H_2O \text{ in Crd(measured)}]/[\text{wt \% } H_2O \text{ in Crd at saturation (Crd*)}].$$

As in the previous diagrams the data obtained at 5·0 kbar, 900°C define a smooth and curved distribution trend (Fig. 7a). Data at 5·0 kbar, 800 and 1000°C (Fig. 7b) essentially follow the same normalized trend apart

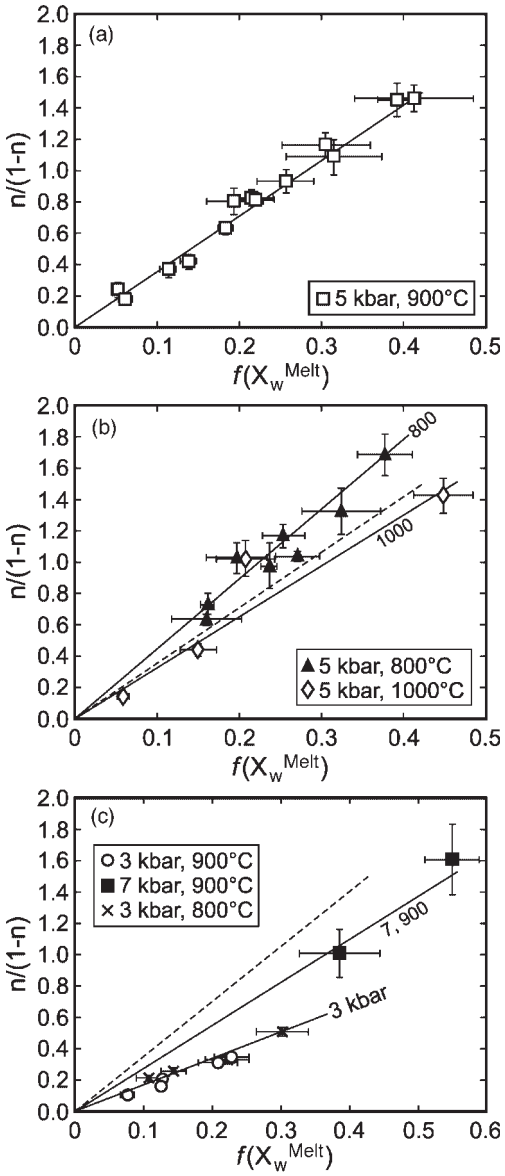

Fig. 8. Water activity parameters for cordierite $[n/(1-n)]$ and melt $f(X_w^{Melt})$ plotted for data obtained at (a) 5·0 kbar, 900°C; (b) 5·0 kbar, 800 and 1000°C; (c) 900°C, 3 and 7 kbar, plus 3·0 kbar, 800°C. $f(X_w^{Melt})$ is based on Burnham (1994) and is equivalent to X_w^2 (melt) at $X_w \leq 0{\cdot}5$, and to $0{\cdot}25\{\exp[(6{\cdot}52 - (2667/T)).X_w]\}$ at $X_w > 0{\cdot}5$. The regressed line through the 5·0 kbar, 900°C data is reproduced in (b) and (c) (dashed line) to facilitate comparisons. Other fitted lines at specific P–T conditions are as labelled.

from the discrepant experiment C16-2, and hence indicate that temperature does not affect the shape and position of the normalized distribution curve. Similarly, isothermal data obtained at 800°C, 3·0 and 5·0 kbar show no effect of pressure on the shape of the normalized distribution curve.

The data obtained at 3·0 kbar, 900°C have not been normalized as fluid saturation was not achieved in experiment C8-1. This is borne out by comparison of our maximum melt H_2O contents with those of Holtz & Johannes (1994), which are in complete agreement (within error) at 5·0 kbar, 900°C; 5·0 kbar, 800°C; and 3·0 kbar, 800°C. In contrast, the melt H_2O content measured at 3·0 kbar, 900°C is 5·94 wt % (C8-1) compared with Holtz & Johannes' saturation value of ~7·4 wt %. Moreover, the measured D_w for this experiment (5·08) is consistent with our other undersaturated Crd–L data obtained at 900°C (Fig. 6b) and 3 kbar (Fig. 6e).

Figure 7 demonstrates that within the range 800–1000°C, 3·0–7·0 kbar the distribution of water between cordierite and granitic melts conforms fairly closely to a single normalized function. This function is represented by the dashed reference curve calculated from the modelling described below and added to each diagram in Fig. 7. The principal determinant of the relative magnitude of the distribution of water between melt and cordierite (D_w) is the system's degree of undersaturation (aH_2O) at the defined P–T condition.

In summary, the data presented in Fig. 5 consistently display the features observed and reported in detail for the 5 kbar, 900°C dataset (Carrington & Harley, 1996). Figure 6 shows that the general form of the D_w–H_2O(Crd) curve at all P–T conditions is one of increasing D_w for cordierite H_2O contents that are <0·75 wt % and >1·0 wt %. D_w values are in the range 5–6 near saturation but are lower in undersaturated conditions, with minima in the range 3·5–4·8 for cordierite with 0·8–1·0 wt % H_2O. Figure 7 demonstrates that the entire Crd–L dataset obtained under polybaric–polythermal conditions follows a consistent pattern that can be described by a single normalized H_2O distribution curve. This is accounted for by the thermodynamic formulations of the incorporation of H_2O into cordierite and melt, as elucidated in the sections below.

THERMODYNAMIC MODELLING OF THE H_2O SYSTEM

The cordierite–melt experimental data can be treated using appropriate thermodynamic models to define the relationships between water activity (aH_2O), D_w and the H_2O contents of cordierite and melt. The thermodynamic models used are described first and then applied to the data to model the relationship between D_w and the H_2O content of cordierite or melt illustrated in Fig. 5. The present results are then integrated with previous experimental data at lower T to develop a revised saturation isohydron set for cordierite in equilibrium with pure H_2O in the P–T range 2–9 kbar and 500–1000°C.

Cordierite–hydrous cordierite

The energetics of hydration of cordierite have been considered by several workers (e.g. Newton & Wood, 1979; Lonker, 1981; Martignole & Sisi, 1981; Kurepin, 1984; Bhattyacharya & Sen, 1985). Largely influenced by the hydration experiments of Mirwald *et al.* (1979), some early models suggested incorporation of up to 1·2 moles of H_2O per formula unit (p.f.u.) of cordierite, achieved under higher-P, lower-T conditions. However, more recent models (e.g. Mukhopadhyay & Holdaway, 1994; Carey, 1995; Skippen & Gunter, 1996) have generally agreed on a one-site, 1 mole mixing model for H_2O incorporation, consistent with both calorimetric measurements (Carey & Navrotsky, 1992) and *ab initio* energy calculations (Winkler *et al.*, 1994). Hence, the analysis of the thermodynamics of hydrous cordierite presented here follows the approach adopted by recent workers (Carey, 1995; Skippen & Gunter, 1996), such that the following relation governs H_2O incorporation into cordierite:

$$\text{Crd(anhydrous)} + H_2O = \text{Crd(hydrous)}. \quad (1)$$

Hereafter, anhydrous cordierite will be denoted by A-Crd and hydrous by H-Crd.

The reaction above then has the following equilibrium expression:

$$K_{eq} = (a_{\text{H-Crd}})/(a_{\text{A-Crd}}.aH_2O) \quad (2)$$

and with the 1 molar model, assuming ideality, $a_{\text{H-Crd}} = n$, where n is the number of moles of H_2O per formula unit of cordierite, and $a_{\text{A-Crd}} = 1 - n$.

Hence

$$K_{eq} = [n/(1 - n)]\text{Crd}.(1/aH_2O) \quad (3)$$

and

$$-RT\ln[n/(1 - n)] + RT\ln(aH_2O) = \Delta H_r - T\Delta S_r + P\Delta V_r. \quad (4)$$

The volume change of reaction can be partitioned into the solids volume change, ΔV_s, and the volume of the vapour phase at the P and T of interest:

$$P\Delta V_r = P\Delta V_s - \int V_{H_2O}dP. \quad (5)$$

The volume change reduces to that of the volatile phase if $\Delta V_s = 0$, a situation considered and modelled by Carey (1995) and Skippen & Gunter (1996). In this paper we will re-examine whether $\Delta V_s = 0$ in the light of the full dataset compiled from our own and previous data, but for analysis of isobaric data this term will be implicit in the retrieved ΔH_r and so will not be considered in the initial modelling. Noting that the integral term in equation (5) is related to the fugacity of H_2O at the P–T of interest, fH_2O, equating with $RT\ln fH_2O$, hence

$$\Delta H_r - T\Delta S_r - RT\ln fH_2O = RT\ln(aH_2O) - RT\ln[n/(1 - n)]. \quad (6)$$

Before any polybaric–polythermal analysis, it is useful to note that at fixed P and T (and therefore also fixed fH_2O at saturation with pure H_2O) the left-hand side of equation (6) is a constant. Rearranging,

$$[\Delta H_r - T\Delta S_r] - RT\ln(aH_2O) = -RT\ln\{[n/(1 - n)]/fH_2O\}. \quad (7)$$

Dividing by RT and taking exponents we obtain

$$a_{H_2O} = \{\exp[(\Delta H_r/RT) - (\Delta S_r/R)]\}.[n/(1 - n)]/fH_2O. \quad (8)$$

Hence, for isobaric–isothermal data aH_2O is proportional to $n/(1- n)$ in cordierite (e.g. Carey, 1995; Skippen & Gunter, 1996). The proportionality constant at a given P–T condition is denoted hereafter as z_w, where w is for 'water'. As is apparent from the derivation above, z_w includes enthalpy and entropy terms that are obtainable from regression of our data and those of Mirwald *et al.* (1979), Boberski & Schreyer (1990), Carey (1995), Skippen & Gunter (1996) and others. Finally,

$$aH_2O = z_w.[n/(1 - n)] \quad (9)$$

with

$$z_w = \{\exp[(\Delta H_r/RT) - (\Delta S_r/R)]\}/fH_2O. \quad (10)$$

At a given P–T condition and unit water activity ($aH_2O = 1$) it follows that z_w is equivalent to

$$(1 - n_{sat})/n_{sat} \quad (11)$$

where n_{sat} is the saturation moles of water in cordierite at that specified P–T condition.

We will first examine how well the isobaric–isothermal experimental data for cordierite can be fitted to the formulation described by (9) and (10), the first instance in which this has been possible by direct measurement. The variation of z_w with pressure and temperature is then evaluated to derive a refined expression for the saturation value of n (n_{sat}) over P–T space and a general relation for n as a function of aH_2O at varied P–T conditions.

Incorporation of H_2O into granitic or peraluminous melts

H_2O can be incorporated into melts through the breaking of Si–O linkages producing –(OH) and (H)O– pairs and as molecular water [see review by Holloway & Blank (1994)]. The latter solubility mechanism, which becomes important at high H_2O contents (e.g. >5 wt % H_2O; McMillan, 1994), may be responsible for H_2O increasingly preferring the melt over cordierite as a residence site, as seen in the D_w data of Fig. 6.

There have been several attempts at modelling the solubility of H_2O in silicate melts (Stolper, 1982; Burnham & Nekvasil, 1986; McMillan & Holloway, 1987; Moore *et al.*, 1995, 1998). Usually these models involve empirical fits to solubility data at saturation and for unit aH_2O for a range of P–T conditions, coupled with compositional terms (e.g. Burnham, 1994; Holloway & Blank, 1994; Moore *et al.*, 1995) to account for the effect of melt network modifiers on H_2O contents. Alternatively, models have been developed that incorporate speciation data (Stolper, 1982) and allow iterative calculation of total H_2O contents at given P–T knowing the speciation between molecular or free H_2O and the H_2O incorporated as a network-breaker (Holloway & Blank, 1994).

The recent and comprehensive model of Papale (1997), which incorporates experimental data to 15 kbar, demonstrates that H_2O solubility in granitic melts is not adequately represented by the Burnham model at high pressures. Although the P–T-dependent parameter k_w defined from our high-P experiments is lower than would be predicted using the Burnham expressions for rhyolite glass (Burnham, 1994), and hence our saturation H_2O contents are higher at pressures of 3–7 kbar, we have used the general formulations of Burnham in the absence of any better high-P model. The critical point of departure for the present analysis, therefore, is that in the granitic liquids at pressures between 3 and 7 kbar we assume that the activity of water can be approximated by the following expressions:

$$aH_2O = k_w(X_w)^2 \text{ (at } X_w \leq 0{\cdot}5) \quad (12a)$$

and

$$aH_2O = 0{\cdot}25k_w\{\exp[(6{\cdot}52 - (2667/T)).X_w]\} \text{ (at } X_w > 0{\cdot}5) \quad (12b)$$

where X_w = (wt % H_2O/18)/{(wt % H_2O/18) + [(100 – wt % H_2O)/MW_{melt}]} is the mole fraction of water in an eight-oxygen unit formula melt, MW_{melt} is the molecular weight of the anhydrous melt when expressed in terms of an eight-oxygen unit, and k_w is a P–T-dependent normalization coefficient. It follows that in the case of isobaric–isothermal data the coefficient k_w is given by [1/$(X_{w,sat})^2$] if $X_{w,sat} < 0{\cdot}5$ or by [1/(0·25{exp[(6·52 – (2667/T)).X_w]})] when $X_{w,sat} > 0{\cdot}5$, where $X_{w,sat}$ is the saturation value of X_w at the P–T conditions of the dataset.

Modelled H_2O distribution (D_w) and its variation with pressure, temperature and aH_2O

In the case of Crd–melt equilibrium, for isobaric–isothermal experimental data obtained from saturated to highly undersaturated conditions aH_2O defined from cordierite must equal aH_2O defined from melt. Hence

$$z_w[n/(1 - n)] = k_w(X_w^2) \text{ (at } X_w \leq 0{\cdot}5) \quad (13a)$$

and

$$z_w[n/(1 - n)] = 0{\cdot}25k_w\{\exp[(6{\cdot}52 - (2667/T)).X_w]\} \text{ (at } X_w > 0{\cdot}5) \quad (13b)$$

and a plot of $n/(1 - n)$ in cordierite versus the two relevant functions in X_w in the melt should yield a straight line with slope, k_w/z_w, that is characteristic for the specified P–T conditions. This relation is depicted for 900°C, 5 kbar data in Fig. 8a and for data obtained at other P–T conditions in Fig. 8b and c. The plots show good linear trends and hence confirm the mutual compatibility of the cordierite and melt hydration models used. Slopes, k_w/z_w, lie in the range 3–6 for the range of P–T conditions accessed directly in the experiments.

Equations (13a) and (13b) can be combined with the relationships between n and weight percent H_2O in cordierite or X_w and weight percent H_2O in melt to determine the variation of D_w as a function of weight percent H_2O in either phase for specified values of k_w/z_w. The theoretical form of D_w so derived is a combination of an inverse and linear function in H_2O, with a calculated minimum region (± 0·2 units) occurring between 0·7 and 0·9 wt % H_2O in cordierite (between 2·5 and 4·5 wt % H_2O in the melt) and the magnitude of D_w then increasing gradually to saturation (Fig. 9). These two features are consistent with the experimental D_w data. The hydration models embodied in equations (13a) and (13b) also predict a rapid asymptotic increase in D_w with decreasing H_2O below 0·2–0·4 wt % in cordierite (<1·2–1·7 wt % H_2O in melt). These marked increases in D_w at low H_2O contents are not readily observed in the experiments, partly because the crystallization of quartz and feldspar in near-solidus H_2O-poor melts hinders the precise measurement of D_w at very low aH_2O. However, the principal limitation is that these effects are predicted to occur at H_2O contents generally less than the minimum possible in a granitic melt at the P–T conditions of most of the experiments: the rapid rise in D_w is largely restricted to an inaccessible region of extreme undersaturation (and low aH_2O) where melting is not possible unless the temperatures are very high. This behaviour is expected to occur at temperatures near the dry granite liquidus (e.g. at 1050°C). Consistent with this prediction, an increase in D_w at low H_2O contents is most evident in the 5 kbar, 1000°C data (Fig. 6d).

The analysis of isobaric–isothermal datasets can be generalized to all P–T conditions through normalization of the variables $n/(1 - n)$ and X_w against their values at saturation at the studied P–T conditions [i.e. $n_{sat}/(1 - n_{sat})$ and $X_{w,sat}$]. This procedure makes the fewest assumptions about the values of k_w and z_w. The bulk of the experimental dataset (all except two points from 36) conforms to a straight-line relation between the melt and cordierite

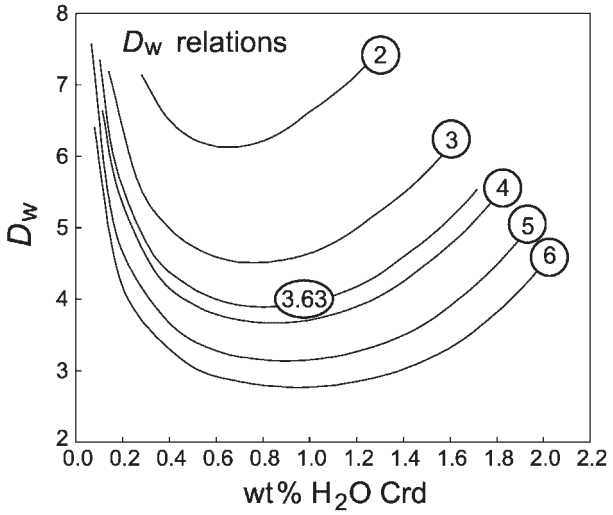

Fig. 9. Modelled variation of D_w with weight percent H_2O in cordierite coexisting with melt, contoured for values of the slope parameter k_w/z_w (see text for definition) that span the P–T conditions of the experiments. The asymmetry in the D_w curves should be noted, with minima in D_w (3·0–4·5 for k_w/z_w = 3–6) occurring at intermediate H_2O contents. The pronounced increases in D_w predicted at very low H_2O contents are not observed in general because the melt is metastable with respect to solid phases (i.e. it would be below its minimum H_2O content for the P–T condition), but this trend is observed in the experiments conducted at 5 kbar, 1000°C (Fig. 6).

aH_2O indicators and supports their applicability to the modelling of D_w relationships over a wide P–T range. Because the modelled D_w curves form a family with the position of any one curve characterized simply by k_w/z_w, they depend only on the relation between $n_{sat}/(1 - n_{sat})$ in cordierite and the functions in $X_{w,sat}$ for the melt at a specified P–T condition and so can be derived from saturation isopleths (isohydrons) for melt and cordierite.

On the basis of existing saturation H_2O isopleths for melts (Holtz & Johannes, 1994; Johannes & Holtz, 1996) and those modelled here for cordierite (see below), k_w/z_w varies between 3·0 and 7·0 across the P–T range 3–7 kbar and 700–1000°C, decreasing with rising T at constant P, and increasing with increasing P at fixed T. For k_w/z_w values between 3·0 and 7·0, modelled D_w lies in the range 2·5–4·5 for those highly undersaturated conditions where cordierite is in equilibrium with a melt that has the minimum possible H_2O content for the specified P–T (Fig. 9). Maximum D_w values, which generally occur at H_2O saturation, are in the range 4·5–6·5 for this degree of variation in k_w/z_w (Fig. 9). The D_w curves generated from the modelling can be used to estimate the H_2O contents of melts coexisting with cordierites of known composition. For example, cordierites containing 1 wt % H_2O could have equilibrated with melts containing 2·5–5 wt % H_2O, depending on P and T, with the higher H_2O content being in melts formed at high T and low P (i.e. low k_w/z_w).

CORDIERITE H_2O SATURATION AND ISOHYDRONS TO 1000°C

The experiments reported here provide six new, directly measured, data points on the saturation H_2O contents of cordierite at 800–1000°C. Furthermore, these are supported by and consistent with several other data points obtained at the same P–T conditions. For example, the saturation H_2O content of cordierite at 5 kbar and 900°C (1·69 ± 0·05 wt % for X_{Mg} = 0·67) is based on two saturation experiments but is also constrained to be in this range by the linear fit to all the other, H_2O-undersaturated, data obtained at this P–T condition.

The new saturation data also access a higher T field than hitherto available for modelling the incorporation of H_2O into cordierite, resulting in a significantly wider $1/T$ interval for fitting experimental hydration data. Accordingly, we have taken the hydration data from previous studies of Mg, Fe and Mg–Fe cordierite (Schreyer & Yoder, 1964; Mirwald *et al.*, 1979; Boberski & Schreyer, 1990; Mukhopadhyay & Holdaway, 1994; Carey, 1995; Skippen & Gunter, 1996), added our own higher-T data, and fitted the entire dataset via a ln K_{eq} vs $1/T$ plot, where ln K_{eq} is evaluated from

$$K_{eq} = [n_{sat}/(1 - n_{sat})]/fH_2O_{(P,T)}. \quad (14)$$

The ln K_{eq} vs $1/T$ plot for all cordierite hydration data is presented in Fig. 10. This does not discriminate subjectively between data or classify data on the basis of measurement technique or run pressure. Although there is significant scatter in ln K_{eq} at temperatures of 800 and 600°C, this is not consistently related to pressure or other intrinsic variables, and linear regression of all the data yields

$$\ln K_{eq} = [4385\ (\pm\ 500)/T] - 11{\cdot}92\ (\pm\ 0{\cdot}55) \quad (r^2 = 0{\cdot}56) \quad (15)$$

where T is in Kelvin (K).

Our preferred fit to the data, however, utilizes 98 points from the 155 available at 40 distinct P–T conditions. The data excluded from this fit are outliers obtained at P–T conditions where two or more other results are mutually compatible and cases in which the relative errors on H_2O measurement are large (>20% relative). This fit, which includes all our data along with all those of Boberski & Schreyer (1990), Mukhopadhyay & Holdaway (1994) and Carey (1995), is as follows:

$$\ln K_{eq} = [4203\ (\pm\ 320)/T] - 11{\cdot}75\ (\pm\ 0{\cdot}33) \quad (r^2 = 0{\cdot}87) \quad (16)$$

where T is in Kelvin (K). This fit yields an average enthalpy change of reaction of $\Delta H_r = -34{\cdot}95$ kJ/mol and entropy change $\Delta S_r = -97{\cdot}69$ J/mol/K for the T range 500–1000°C.

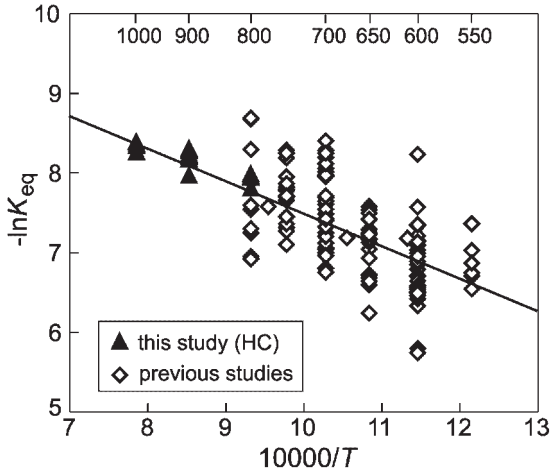

Fig. 10. Plot of –ln K_{eq} vs 10 000/T for the hydration of cordierite in equilibrium with pure H_2O. ▲, saturation data obtained in this study at 800, 900 and 1000°C; ◇, data from all other sources as outlined in the text. This plot presents all 155 data points, but the best-fit line (continuous line) is regressed through 98 data points that exclude the far outliers where duplicate data are available, several points that have large analytical uncertainties, and points obtained at extreme P conditions ($\geq$9 kbar).

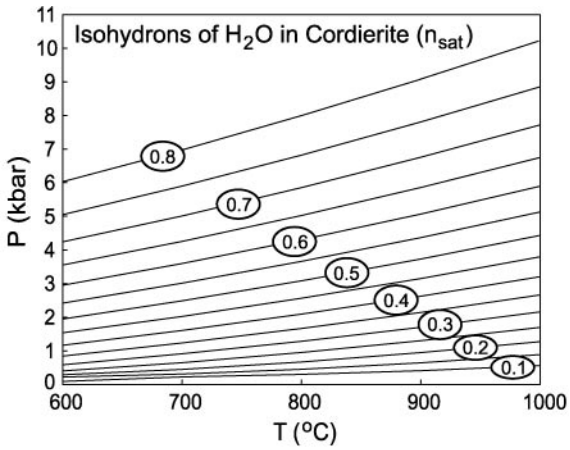

Fig. 11. Pressure–temperature diagram contoured with the isohydrons of H_2O in cordierite coexisting with pure H_2O fluid. The isohydrons, expressed in terms of molecules of H_2O per 18 oxygen formula unit (i.e. n_{sat}), are derived from equation (16) and incorporate experimental data from previous studies and the new data of this study at 800–1000°C.

To assess whether the assumption of $\Delta V_s = 0$ is reasonable we tested correlations of ln K_{eq} against P for isothermal datasets obtained in previous experimental studies as well as those presented here. Whereas data at 800°C and 700°C show moderate correlations of ln K_{eq} with P and yield similar d(ln K_{eq})/dP slopes of 0·88 J/kbar, any P dependence of data at 600°C, 750°C, 900°C and 1000°C is within the errors of measurement. In agreement with Carey (1995), we conclude that the extraction of a ΔV_s term is not warranted, based on the existing hydration data and given the uncertainties in these data.

Recent heat capacity data for cordierite indicate that C_p of hydrous cordierite (H-Crd) is higher than that of anhydrous cordierite (A-Crd) by ~8·3 J/mol/K (Carey & Navrotsky, 1992). Holland & Powell (1998) have accordingly fitted cordierite hydration data over the T range 500–800°C (i.e. excluding the data presented here) with the ΔC_p of reaction included, to derive estimates for ΔH_{298} and ΔS_{298}. Their retrieved values of −41·8 kJ/mol and −109·0 J/K/mol respectively are within error of our estimates of ΔH_{298} (−41·97 kJ/mol) and ΔS_{298} (−109·11 J/K/mol) obtained when the ΔC_p from Carey & Navrotsky (1992) is included in the regression of the 500–1000°C data. In this case the best-fit result is

$$\ln K_{eq} = [5048\ (\pm\ 400)/T] - 13{\cdot}12\ (\pm\ 0{\cdot}30) - [(T - 298{\cdot}15)/T] + \ln(T/298{\cdot}15)\ (r^2 = 0{\cdot}77) \quad (17)$$

which has a significantly lower r^2 than the simple fit (16) that neglects the ΔC_p term.

In the light of the errors inherent in the experimental data we prefer the simpler fit given in equation (16) for direct calculation of saturation isohydrons of H_2O in cordierite over the T range 500–1000°C. The isohydrons thus produced, expressed in terms of molecules of H_2O per 18-oxygen anhydrous cordierite formula unit (i.e. n_{sat}), are presented in Fig. 11 and compared with those presented by Skippen & Gunter (1996) and calculated using Holland & Powell (1998) in Fig. 12. The geohydrometer of Skippen & Gunter (1996) yields higher H_2O contents in cordierite than predicted from our isohydrons at all P–T conditions, with the greatest differences occurring at lower pressures and for lower temperatures (2–4 kbar, 600–700°C; Fig. 12a). The two isohydron sets are within error ($\pm$0·015 p.f.u.) at high temperatures. Isohydrons calculated from Holland & Powell (1998) are lower than the best-fit isohydrons produced here (Fig. 12b), but only by 0·005–0·01 p.f.u. over most of the P–T range considered. Such differences equate to differences in H_2O of only $\pm$0·02–0·04 wt % and are within the errors of measurement of H_2O contents in cordierite using SIMS and other methods (usually > $\pm$0·05 wt %). In summary, the isohydron set presented in Fig. 11 defines the P–T dependence of the hydration of cordierite in the presence of pure H_2O and is consistent with the best available experimental data as modelled in previous studies as well as with our new data at 800–1000°C. Equation (16), or the isohydrons of Fig. 11, can be used in concert with measured contents of H_2O in natural cordierites and independent estimates of the P–T conditions of equilibration to calculate $a$$H_2O$ via equations (9), (10) or (11). Examples of such applications are presented below.

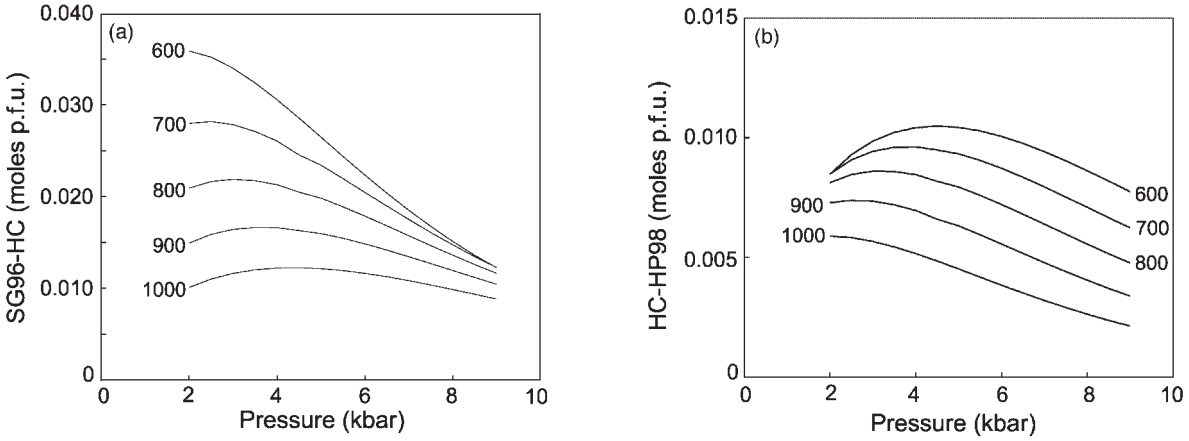

Fig. 12. Difference diagrams comparing the hydration state of cordierite derived from equation (16) (HC) with those derived based on Skippen & Gunter (1996) [SG96 in (a)] and calculated using Holland & Powell (1998) [HP98 in (b)]. Differences in n_{sat} (in molecules per formula unit) are plotted against pressure and contoured for different temperature conditions. The results of Skippen & Gunter (1996) yield slightly higher H_2O contents than predicted from equation (16), whereas those of Holland & Powell (1998) give similar H_2O contents to those defined by equation (16), being lower by 0·005–0·01 molecules p.f.u., equivalent to differences of only 0·02–0·04 wt % H_2O.

APPLICATIONS TO MELTING AND HIGH-TEMPERATURE FLUID PROCESSES

D_w for H_2O-saturated conditions and the wet granite solidus

Superimposition of the saturation isohydrons for cordierite on the isopleths for maximum H_2O contents in peraluminous granitic melts allows calculation of k_w/z_w over the P–T field of melt stability and also direct determination of the D_w at saturation [$D_{w(sat)}$]. Contours of $D_{w(sat)}$ are presented along with cordierite and melt saturation isohydrons and isopleths in Fig. 13a. Over the P–T field 1–8 kbar and 650–900°C, $D_{w(sat)}$ varies in the range 4·1–6·2. The slightly steeper positive slopes of the cordierite isohydrons compared with melt saturation H_2O isopleths cause $D_{w(sat)}$ to increase with rising temperature and pressure over most of the P–T range of mid- and deep-crustal melting, but the $D_{w(sat)}$ contours switch from these negative dP/dT slopes to positive dP/dT at pressures <2 kbar. $D_{w(sat)}$ only varies between 4·2 and 5·0 along the water-saturated solidus in the NKFMASH or simplified granite system, for pressures in the range 1–6 kbar. The experimental data indicate that an average D_w of 4·3 $\pm$ 0·2 is appropriate for cordierite crystallized in the majority of wet- or near-saturated granites that are emplaced at shallow crustal pressures and exhibit andalusite–sillimanite type contact metamorphism.

D_w for H_2O-undersaturated conditions in the realm of dehydration-melting

In the KFMASH system at temperatures higher than 800°C the majority of reactions involving cordierite will be dehydration-melting reactions (e.g. Carrington & Harley, 1995), and in such cases the cordierite will be constrained by the highly H_2O-undersaturated melts produced through dehydration melting to have H_2O-undersaturated compositions (Stevens *et al.*, 1995; Carrington & Harley, 1996). In such circumstances, cordierite H_2O contents will be buffered through the exchange equilibrium

$$H_2O(Crd) = H_2O(L) \qquad (18)$$

for which we have now defined the distribution coefficient D_w, and its variation with the absolute H_2O contents of the melt. Unless appropriate chemical constituents other than H_2O available from biotite and other hydrous reactant phases are exhausted first, the H_2O content of the melt will closely approach the minimum attainable for the specified P–T conditions of dehydration-melting and melt production will be maximized (Stevens & Clemens, 1993; Johannes & Holtz, 1996). Hence, the dehydration-melting KFMASH grids of Carrington & Harley (1995), contoured for X_{Mg} isopleths by Harley (1998*a*), can also be contoured for the H_2O content of cordierite in melt-bearing assemblages provided that the melt minimum-H_2O contours are independently estimated.

In Fig. 13b are plotted isopleths of the minimum H_2O contents of granitic melts for the P–T conditions of

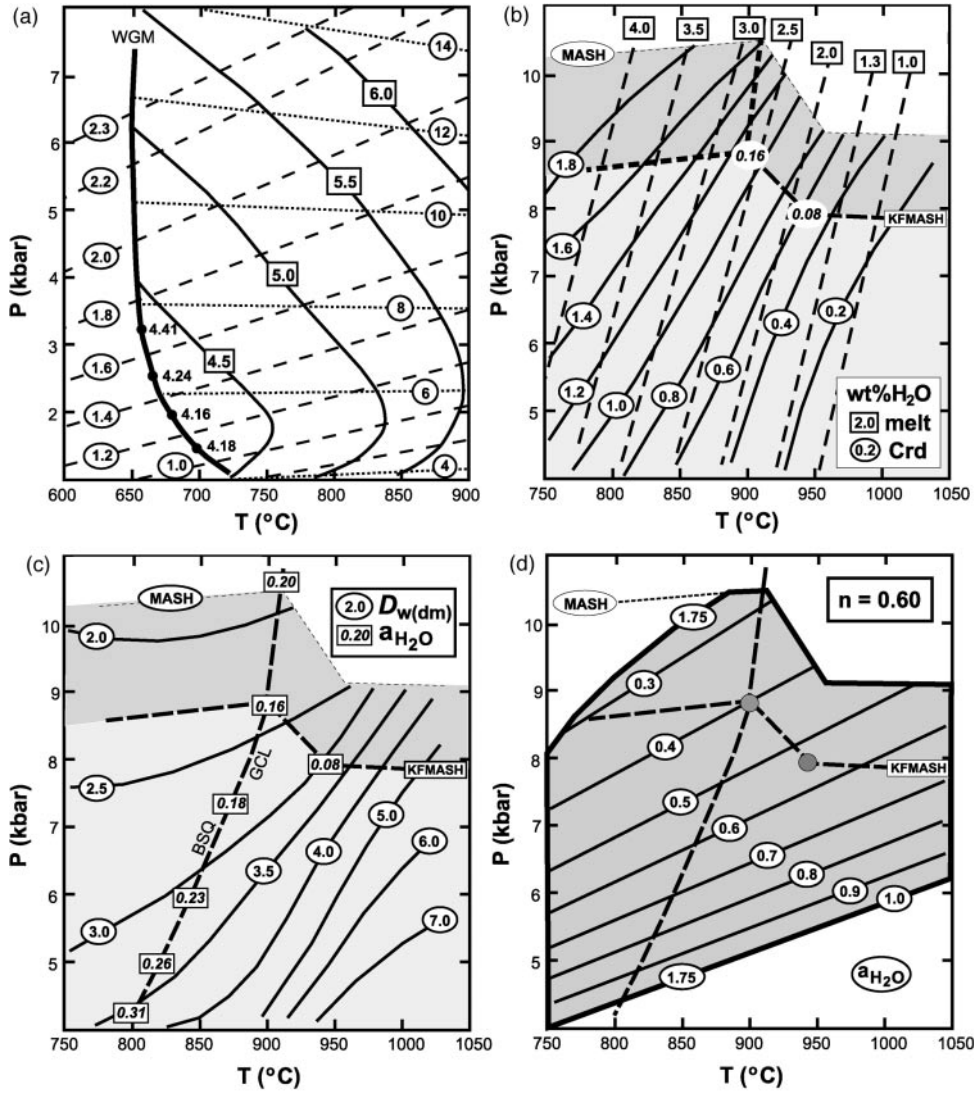

Fig. 13. (a) Contoured P–T diagram depicting cordierite–melt H_2O relationships at $aH_2O = 1$. The weight percent contours are of melt H_2O contents (dotted, after Holtz & Johannes, 1994) and cordierite H_2O contents (dashed, this study) in equilibrium with free H_2O; $D_{w(sat)}$ contours are continuous lines. Wet granite solidus represents the minimum temperature conditions under which cordierite and H_2O-saturated melt can coexist. (Note the change in slope of the $D_{w(sat)}$ contours at ~ 2 kbar and the near-constant value of 4·3 for $D_{w(sat)}$ along the wet solidus curve.) (b) Contoured P–T diagram depicting cordierite–melt H_2O relationships for conditions where the melt has its minimum possible H_2O content at P and T (i.e. variable aH_2O). Contours of minimum melt H_2O content (in wt %) are after Holtz & Johannes (1994) and this study. Contours of cordierite H_2O contents (wt %) are based on the D_w–aH_2O relationships defined in this study. Other lines in this figure are the approximate positions of KFMASH (heavy dash) and MASH (fine dash) reactions that limit cordierite + garnet stability in KFMASH and cordierite stability in MASH, after Carrington & Harley (1995), with KFMASH invariant points labelled for aH_2O (italics). (c) P–T diagram similar to (b) but contoured for $D_{w(dm)}$, where this parameter is the D_w relevant to dehydration melting equilibria. (Note that $D_{w(dm)}$ always has a positive dP/dT and increases towards high-T, low-P conditions.) Dashed curve labelled BSQ_GCL is the reaction Bt + Sill + Qz = Grt + Crd + Kfs + L as defined in the KFMASH system by the experiments of Carrington & Harley (1995), annotated with aH_2O (decimals in rectangles); cordierite H_2O contents along and near this reaction are in the range 1·1–0·9 wt %. Other lines as in (b). (d) P–T diagram illustrating the stability field over which a cordierite of specified H_2O content, in this case 1·75 wt % H_2O ($n = 0{\cdot}60$), can coexist with melt or melt + fluid (shaded field). Contours are of aH_2O (decimals in ellipses). The stability field is bounded by the $aH_2O = 1$ line (Crd + L + H_2O equilibrium) at lower P and by a line at higher P that reflects the minimum T at which melt can coexist with the cordierite. Other lines as in (b); ●, KFMASH invariant points after Carrington & Harley (1995).

dehydration-melting in KFMASH. These melt (L) H_2O isopleths are modified from Holtz & Johannes (1994) and Johannes & Holtz (1996) for peraluminous melts in KFMASH and are consistent with minimum H_2O content data reported by Carrington & Harley (1996) and presented in this work. The diagram is also contoured

with isohydrons (in wt %) of H_2O in cordierite coexisting with such melts in the assemblages cordierite + garnet + sillimanite + quartz + K-feldspar + melt (higher-T) and cordierite + biotite + sillimanite + quartz + K-feldspar + melt (lower-T). These isohydrons have been obtained by combining the melt minimum-H_2O isopleths with the P–T-dependent D_w functions for melt–cordierite partitioning developed here and correcting the weight percent H_2O in cordierite for the X_{Mg} of the cordierite present in the assemblage at the relevant P–T condition. The isohydrons can also be positioned by calculating aH_2O from the melt isopleths and then solving for n(Crd) at that aH_2O and the given P–T using expressions (9), (11) and (16) given above.

The cordierite H_2O-isopleths in this situation (i.e. in univariant and divariant dehydration-melting) have much steeper positive dP/dT slopes than isohydrons in the saturated cases (34–75 bar/°C compared with 2·5–10 bar/°C) because they are governed by the relation (18) and because the melt minimum-H_2O isopleths are strongly temperature, rather than pressure, sensitive. In dehydration-melting the cordierite isohydrons are slightly shallower than the melt isopleths (dP/dT = 84 bar/°C for melts; Fig. 13b), whereas in the case of H_2O-saturated melting (Fig. 13a) the isohydrons are steeper than the saturation H_2O isopleths in the melt. This reflects a marked difference in the P–T behaviour of D_w when melts with the lowest H_2O contents attainable are compared with the saturated case.

As illustrated in Fig. 13c, D_w values relevant to dehydration melting [hereafter denoted $D_{w(dm)}$] in the T range 750–900°C vary between 2·6 and 5·0, with the lowest values calculated at high-P, lower-T conditions where $D_{w(sat)}$ is high (e.g. 8 kbar, 750°C: $D_{w(sat)}$ = 6·0 compared with $D_{w(dm)}$ = 2·6). $D_{w(dm)}$ contours have shallow to steep positive dP/dT slopes and always increase with rising temperature. As a consequence, very high $D_{w(dm)}$ values of 6–8 are attained only at high-T, low-P conditions where the H_2O contents in each phase are the range in which the D_w curves display asymptotic behaviour (Fig. 9).

Of particular interest are the variations in cordierite H_2O contents, aH_2O and $D_{w(dm)}$ calculated along the dehydration-melting or vapour-absent melting reaction

$$Bt + Sill + Qtz = Grt + Crd + Kfs + L$$

(Fig. 13c). This reaction, its related divariants, and more complex-system analogues are inferred to have been the prime controls on melting and the development of migmatitic granulites in many high-grade terrains, as described in the Introduction. Hence the H_2O contents of cordierites in such migmatitic granulites would, ideally, correspond to predictions from the intersections between this reaction (or its analogues in more complex systems) and the cordierite isopleths of Fig. 13b. The simplest testable result is that cordierite H_2O contents along the reaction as positioned here are 1·1–0·9 wt % over a very large range in pressure (8·8 to 4 kbar) and only decrease weakly as pressure decreases (Fig. 13b and c). $D_{w(dm)}$ increases from 2·4 to 3·7 as pressure decreases from 9 to 4 kbar along this reaction, and will converge with $D_{w(sat)}$ (= 4·3–4·1) at the low pressures where the reaction may intersect the wet granite solidus. As expected from theoretical arguments (e.g. Stevens & Clemens, 1993), aH_2O increases as pressure decreases along the reaction, from 0·16 at ~9 kbar to >0·31 at 4 kbar when calculated using the modelled cordierite H_2O contents coupled with equations (9), (10) and (16). The biotite dehydration-melting reaction emanating to higher pressures than the invariant point shows a calculated increase in aH_2O with pressure (from 0·16 to 0·20), consistent with Schreinemakers' rules, as its metastable extension, rather than stable portion, intersects the wet granite solidus at low pressure.

P–T stability of cordierite with fixed H_2O content

Figure 13d uses the data from Fig. 13a and b and the models formulated in equations (9) and (16) to illustrate the stability region for a cordierite with a specific weight percent H_2O content. In this example the number of molecules of H_2O per cordierite formula unit is 0·60; for an X_{Mg} of 0·65 this equates to 1·75 wt % H_2O in the cordierite. This diagram is contoured for aH_2O, ranging from the minimum possible at high P–T conditions where the cordierite is in equilibrium with a H_2O-undersaturated dehydration-melt (from Fig. 13b) to unit aH_2O, where the cordierite (and melt) would be H_2O saturated and in equilibrium with pure water (Fig. 13a). Hence, the shaded field represents the P–T range in which a cordierite with 1·75 wt % H_2O is stable and can, in principle, in the absence of any fluid-related perturbations and exchange or mineral reactions retain this H_2O content. In the absence of a fluid or melt phase with which to exchange or equilibrate, and provided porosity is trivial, there is no necessity for the cordierite, once formed, to either lose or gain H_2O as conditions change within this P–T field. For example, a cordierite with 1·75 wt % H_2O formed at 7 kbar and 900°C could be subjected to near-isothermal decompression through 2 kbar under fluid- and melt-absent conditions before becoming 'oversaturated' and likely to lose H_2O from its channels.

As is emphasized from inspection of Fig. 13d, there is no unique line in P–T space that defines the stability of a cordierite with a specific H_2O content. Even in the absence of CO_2, at high temperatures where melt is present cordierite with a specific H_2O content can be

formed over a rather large *P–T* field depending on the imposed aH_2O. In the example shown (Fig. 13d) there is a 5 kbar difference, at 850°C, between the pressure at which the cordierite with 1·75 wt % H_2O would form coexisting with aqueous fluid and the pressure at which it would form in equilibrium with a melt containing 3·5 wt % H_2O.

Migmatites and metamorphism: aH_2O estimates and melt H_2O contents

The cordierite hydration calibration developed here, and the D_w relationships defined from our experiments and modelling, can, in principle, be used to calculate the aH_2O of melting and metamorphism in high-grade metamorphic terrains characterized by cordierite migmatites and applied to infer the H_2O contents of the melts formerly present during the metamorphism. Conversely, where the *P–T–*aH_2O conditions of melting and metamorphism are well known from independent equilibria, cordierite H_2O contents predicted from our modelling can be compared with measured contents to evaluate the role of H_2O addition into or leakage from cordierite subsequent to melting and metamorphism. Table 5 presents a summary of cordierite data from selected migmatite terrains and cordierite-bearing granites and pegmatites. The cordierite volatile content data in most of the cited cases have been obtained using SIMS analysis with negative secondary ions, as described in a previous section and by Carrington & Harley (1996).

Cordierite occurs as a euhedral to subhedral phase in many low- and medium-pressure migmatites found in both regional and contact metamorphism (e.g. Waters & Whales, 1984; Stevens & Clemens, 1993; Carrington & Harley, 1995). The common occurrence of cordierite as single grains and grain clusters in leucosome veins and patches, as inclusion-free grains along mesosome–leucosome contacts (e.g. Harley, 1994; Fitzsimons, 1996), and as inclusion-free rinds overgrowing sillimanite- or biotite-bearing cordierite cores (e.g. Buick *et al.*, 1998) is consistent with its generation through dehydration-melting reactions of the form

$$\mathrm{Bt} + \mathrm{Sil} + \mathrm{Qz} \pm \mathrm{Plag} = \mathrm{Crd} \pm \mathrm{Kfs} + \mathrm{L}$$

and related reactions that may progress during melt crystallization and wall-rock reaction.

The H_2O contents of cordierites from several examples of such migmatite occurrences, some of which will be described in more detail elsewhere, are presented in Table 5. The data are coupled with independent *P–T* estimates to allow calculation of apparent aH_2O, D_w, and hence the nominal H_2O content (in wt %) of coexisting granitic melt, using equations (9), (10) and (16) as given above. Cordierites from several lower-*P* migmatitic granulite areas (<5 kbar, Table 5) yield aH_2O estimates of between 0·2 and 0·6 and melt H_2O contents between 2·5 and 4 wt % at temperatures of 675–800°C. The higher aH_2O conditions tend to be calculated in cases where extensive segregated leucosomes and granitic sheets occur (e.g. Mt Stafford, Argentina, Kimberly region of West Australia), comparable with aH_2O estimates from cordierites in many leucogranites and well-segregated pegmatites (Table 5). For example, cordierite leucogranite from Beatenally quarry, in the Proterozoic Northampton Block of Western Australia, contains 1·3 wt % H_2O and implies $\sim$4·6 $\pm$ 0·4% H_2O in the coexisting granite liquid at an aH_2O of 0·44 $\pm$ 0·04, whereas a restitic cordierite–spinel–sillimanite gneiss xenolith in granite from the same locality suggests a much lower aH_2O (0·12 $\pm$ 0·03) and potential melt H_2O content (1·9 $\pm$ 0·4 wt %) if it equilibrated at the same *P–T* conditions. In this example, and in other cases where cordierite remains in contact with segregated melt, it is considered likely that the higher H_2O contents and aH_2O attained in the granites and pegmatites reflect the addition or uptake of H_2O into cordierite as the melt increases in its H_2O content during crystallization following segregation and ponding.

The well-developed migmatites and leucogranites described by Smith (1996) from the Cretaceous Fosdick Complex of Antarctica contain cordierites whose H_2O contents indicate aH_2O (0·36 $\pm$ 0·05) and melt H_2O contents (3·9 $\pm$ 0·5 wt %) that are consistent with biotite dehydration-melting at the inferred temperature conditions of the metamorphic event and hence argue against significant H_2O leakage or addition into the cordierites subsequent to the melting event. The same conclusions can be drawn from various other examples distinguished in Table 5. For example, at Mount Stafford in the Arunta Complex (Vernon *et al.*, 1990; Greenfield *et al.*, 1998) cordierite in granitic leucosomes contains $\sim$1 wt % H_2O (Table 5). Using our hydration model, at 2·5 kbar and 650°C we obtain aH_2O of 0·4 from these cordierites, and calculate 4·2 wt % H_2O in the coexisting melts, reasonably consistent with phase equilibria constraints (Greenfield *et al.*, 1998).

Cordierite is often considered to be susceptible to post-formation leakage from the relatively 'open' channels (e.g. Aines & Rossman, 1984; Mirwald *et al.*, 1986) and it is possible that in many cases the peak volatile contents are not retained. In accord with this, some of the migmatite examples in Table 5 may be interpreted to have experienced H_2O loss as their preserved H_2O contents yield 'melt' H_2O contents that are too low to be consistent with dehydration-melting at the independently inferred *P–T* conditions. Sample 9017, a cordierite–quartz–feldspar patch leucosome from the Reynolds Range, Arunta Complex, central Australia (Buick *et al.*,

Table 5: Cordierite water activity calculations and melt H_2O contents

Area	*P* (kbar)	*T* (°C)	$H_2O_{(Crd)}$ (wt %)	D_w	$H_2O_{(m)}$ (wt %)	aH_2O	$CO_{2(Crd)}$ (wt %)	Reference and assemblage
Migmatites								
Mt Stafford	2·5	800	0·85	4·4	3·6	0·51	0·03	Greenfield *et al.* (1998)
(nebulites)								Crd–And–Sil–Spl–Qz
Kimberly region	3·5	775	0·62	3·8	2·4	0·22	0·13	(Warren)*
(contact melts)								Crd–Sil–Mt–Crn
Kimberly region	3·5	775	1·10	3·8	4·1	0·47	0·46	(Watt)*
(granite/migmatites)								Crd–Kfs–Qz + Bt
Reynolds Range	5·0	775	0·69	3·2	2·2	0·16	0·23	(Harley)*
(cordierite Ck)								Crd–Sil–Qz
Fosdick	5·0	750	1·25	3·1	3·9	0·36	0·26	Smith (1996)
(migmatites)								Crd–Grt–Kfs–Bt–Qz
Madagascar	5·0	850	0·29	4·4	1·3	0·06	0·53	(Nicollet)*
(migmatite)								Crd–Qz
Northampton	5·0	800	0·53	3·5	1·9	0·12	0·65	(Harley)*
(restite)								Crd–Sil–Spl–Qz
Prydz Bay	5·5	825	0·50	3·5	1·8	0·10	0·71	(Harley)*
(migmatites)								Crd–Sil–Grt–Spl–Qz
Strangways	6·0	800	0·69	2·9	2·0	0·12	0·02	(Harley)*
(Phlogopite Mine)								Crd–Opx–Kfs–Qz
Strangways	6·0	800	1·15	2·9	3·4	0·26	0·42	(Harley)*
(Edwards Ck)								Crd
Rauer Islands	8·0	920	0·70	2·9	2·0	0·10	0·06	Harley (1998*b*)
(Mather)								Crd–Grt–Opx–Sil–Kfs
Granites and pegmatites								
Reynolds Range	3·3	675	0·93	3·2	3·0	0·33	0·73	(Buick)*
(pegmatite)								Crd–Qz
Argentina	3·5	700	1·18	3·4	4·0	0·47	0·31	(Rapela)*
(cordieritite)								Crd–Bt–Kfs–Musc
Northampton	5·0	800	1·30	3·5	4·6	0·44	0·63	(Harley)*
(granite)								Crd–Kfs–Qz

All volatile analyses carried out in SIMS negative mode using procedures outlined in the text and by Carrington & Harley (1996) and Harley (1994). Weight percent data are averages of 6–12 cordierite analyses on either one or several samples from the given locality. Details to be presented elsewhere.
*Unpublished cordierite volatile data by Harley, collected from 1992–1998, material provided by researcher whose name is given in parentheses. *P–T* data based on original references or estimates provided by co-workers.
And, andalusite; Bt, biotite; Crd, cordierite; Crn, corundum; Grt, garnet; Kfs, K-feldspar; Mt, magnetite; Musc, muscovite; Opx, orthopyroxene; Qz, quartz; Sil, sillimanite; Spl, spinel; melt is denoted by the subscript m.

1998), yields an aH_2O of only 0·16 and melt H_2O contents (2·2 wt %) that are too low for the specified peak temperatures of 775°C. Likewise, several cordierites from garnet-bearing migmatites from Prydz Bay, East Antarctica, imply apparent melt H_2O contents of only 1·6–2·0 wt %. These are substantially less than the 3–3·5 wt % minima required for granitic melts at 5·5–6·5 kbar and 825–850°C, the inferred conditions of melting in this case (Fitzsimons, 1996). Cordierite in a leucosome from Madagascar, supplied by C. Nicollet, displays the same type of H_2O deficiency in comparison with melt H_2O requirements and again indicates that volatile loss from cordierite in leucosomes has to be considered when evaluating the measured H_2O data. In all these cited examples the alternative explanation of the low phase H_2O contents and aH_2O would be that the peak temperature estimates used for the rock suites are lower than those at which cordierite and melt equilibrated at or near

the metamorphic peak, a possibility that requires further evaluation using independent thermometry and assemblage constraints in each case.

Two orthopyroxene-bearing migmatitic samples provide good evidence for low aH_2O conditions related to high-T melting. Sample 9052, a cordierite–orthopyroxene segregation in a garnet-bearing semipelitic gneiss from the Strangway Range of the Arunta Complex, suggests melting at aH_2O of 0·12 to yield a melt with 2 wt % H_2O, at ~900°C. Ultrahigh-temperature melting and migmatization at Mather Peninsula in the Rauer Islands (Harley, 1998*b*) produced orthopyroxene + sillimanite + garnet and locally cordierite at P–T conditions of 8–9 kbar and 920–950°C. The aH_2O (0·1) and melt H_2O content (2 wt %) estimated from cordierite H_2O data in this example are consistent with values expected from independent experimental data at these P–T conditions (Carrington & Watt, 1995).

In many of the cases listed in Table 5 and considered above CO_2 is an additional important volatile in cordierite, ranging from >0·7 wt % (e.g. Prydz Bay, Reynolds Range) to more typical contents in the range 0·1–0·4 wt %. It is beyond the scope of this contribution to analyse and review the impact of CO_2 on the D_w relationships developed from the H_2O-only study. However, on the basis of experiments in the H_2O–CO_2 system (Thompson *et al.*, 2001) the effect of CO_2 on D_w at a given cordierite H_2O content can be demonstrated to be negligible.

CONCLUSIONS

Experimental study of the distribution of H_2O between cordierite and coexisting granitic melt demonstrates that this distribution, D_w, is a predictable function of P, T and aH_2O. D_w generally lies in the range 2·5–6·0 and at any selected P–T condition will vary depending on cordierite H_2O content, with a minimum region corresponding to low to moderate aH_2O. The H_2O-undersaturated experiments prove that cordierite can have a range of equilibrium H_2O contents at any specified P–T condition in the regime of melting, up to maxima defined by the H_2O-saturated, fluid-present, system.

The isothermal–isobaric H_2O content data for melt and cordierite are mutually consistent with simple solution models and, when coupled with the measured H_2O data for cordierite in the saturated system, allow refinement of estimates for the thermodynamic parameters for cordierite hydration to 1000°C. The isohydron set so derived is similar to those recently produced by Skippen & Gunter (1996) over a smaller temperature range and within error of that which would be produced using the internally consistent dataset of Holland & Powell (1998).

The D_w–P–T–aH_2O relations derived in this study allow calculation of the equilibrium H_2O contents of cordierite coexisting with melts with given H_2O at specified P and T, and vice versa, estimation of aH_2O and cordierite–melt H_2O contents along selected melting equilibria, calculation of H_2O isohydrons for cordierite produced with melts formed through di- and multivariant dehydration-melting processes, and independent estimation of aH_2O in cordierite-bearing migmatites, granites and granulite terrains. Such calculations provide a framework for examining the effect of H_2O in cordierite upon melt production in high-grade metamorphism. They also demonstrate that whereas some cordierite migmatites formed under aH_2O conditions consistent with biotite dehydration-melting, the H_2O contents of other high-grade cordierites may reflect post-melting processes including H_2O uptake during melt crystallization and H_2O leakage following melt removal.

ACKNOWLEDGEMENTS

Our thanks go to the following people: John Craven and Richard Hinton for assistance with SIMS analysis; Simon Burgess and Peter Hill for assistance with EMP analysis; Tim Hopkins and David Plant for assistance with SEM analysis; Volker Schenk, Dave Mattey, and Tony Fallick for analysis of cordierite standards; Francois Holtz for the provision of SIMS melt standards; Dave Mattey and Ian Fitzsimons for cordierite evacuation; and Pauline Thompson for discussions. Our thanks are due also to Dave Pattison, Gary Stevens and an anonymous reviewer for perceptive and detailed reviews that, it is hoped, have improved the clarity of this paper. This research was funded by the UK Natural Environment Research Council through grant GR3/09099 to S.L.H.

REFERENCES

Aines, R. D. & Rossman, G. R. (1984). The high-temperature behavior of water and carbon dioxide in cordierite and beryl. *American Mineralogist* **69**, 319–327.

Armbruster, Th. & Bloss, F. D. (1980). Channel CO_2 in cordierites. *Nature* **286**, 140–141.

Armbruster, Th. & Bloss, F. D. (1982). Orientation and effects of channel H_2O and CO_2 in cordierite. *American Mineralogist* **67**, 284–291.

Armbruster, Th., Schreyer, W. & Hoefs, J. (1982). Very high CO_2 cordierite from Norwegian Lapland: mineralogy, petrology, and carbon isotopes. *Contributions to Mineralogy and Petrology* **81**, 262–267.

Barbey, P., Macaudiere, J. & Nzenti, J. P. (1990). High-pressure dehydration melting of metapelites: evidence from the migmatites of Yaoundé (Cameroon). *Journal of Petrology* **31**, 401–427.

Bhattacharya, A. & Sen, S. K. (1985). Energetics of hydration of cordierite and water barometry in cordierite-granulites. *Contributions to Mineralogy and Petrology* **89**, 370–378.

Bhattacharya, A. & Sen, S. K. (1986). Granulite metamorphism, fluid buffering, and dehydration melting in the Madras charnockites and metapelites. *Journal of Petrology* **27**, 1119–1141.

Boberski, C. & Schreyer, W. (1990). Synthesis and water contents of Fe^{2+}-cordierites. *European Journal of Mineralogy* **2**, 565–584.

Buick, I. S., Cartwright, I. & Harley, S. L. (1998). The retrograde *P–T–t* path for low-pressure granulites from the Reynolds Range, central Australia: petrological constraints and implications for low-*P*/high-*T* metamorphism. *Journal of Metamorphic Geology* **16**, 511–529.

Burnham, C. W. (1994). Development of the Burnham model for prediction of H_2O solubility in magmas. In: Carroll, M. R. & Holloway, J. R. (eds) *Volatiles in Magmas. Mineralogical Society of America, Reviews in Mineralogy* **30**, 123–129.

Burnham, C. W. & Nekvasil, H. (1986). Equilibrium properties of granitic pegmatite magmas. *American Mineralogist* **71**, 239–263.

Carey, J. W. (1995). A thermodynamic formulation for hydrous cordierite. *Contributions to Mineralogy and Petrology* **119**, 155–165.

Carey, J. W. & Navrotsky, A. (1992). The molar enthalpy of dehydration of cordierite. *American Mineralogist* **77**, 930–936.

Carrington, D. P. & Harley, S. L. (1995). Partial melting and phase relations in high-grade metapelites: an experimental petrogenetic grid in the KFMASH system. *Contributions to Mineralogy and Petrology* **120**, 270–291.

Carrington, D. P. & Harley, S. L. (1996). Cordierite as a monitor of fluid and melt water contents in the lower crust: an experimental calibration. *Geology* **24**, 647–650.

Carrington, D. P. & Watt, G. R. (1995). A geochemical and experimental study of the role of K-feldspar during water-undersaturated melting of metapelites. *Chemical Geology* **122**, 59–76.

Clemens, J. D. & Vielzeuf, D. (1987). Constraints on melting and magma production in the crust. *Earth and Planetary Science Letters* **86**, 287–306.

Fitzsimons, I. C. W. (1994). Cordierite migmatites from East Antarctica: geochemical constraints on volatile distribution during crustal anatexis. *Mineralogical Magazine* **58a**, 274–275.

Fitzsimons, I. C. W. (1996). Metapelitic migmatites from Brattstrand Bluffs, east Antarctica—metamorphism, melting and exhumation of the mid-crust. *Journal of Petrology* **37**, 395–414.

Goldman, D. S., Rossman, G. R. & Dollase, W. A. (1977). Channel constituents in cordierite. *American Mineralogist* **62**, 1144–1157.

Greenfield, J. E., Clarke, G. L. & White, R. W. (1998). A sequence of partial melting reactions at Mt Stafford, central Australia. *Journal of Metamorphic Geology* **16**, 363–378.

Harley, S. L. (1989). The origins of granulites: a metamorphic perspective. *Geological Magazine* **126**, 215–247.

Harley, S. L. (1994). Cordierite as a sensor of fluid and melt distribution in crustal metamorphism. *Mineralogical Magazine* **58a**, 374–375.

Harley, S. L. (1998*a*). On the occurrence and characterization of ultrahigh-temperature (UHT) crustal metamorphism. In: Treloar, P. J. & O'Brien, P. (eds) *What Controls Metamorphism and Metamorphic Reactions? Geological Society, London, Special Publications* **138**, 75–101.

Harley, S. L. (1998*b*). Ultrahigh temperature granulite metamorphism (1050°C, 12 kbar) and decompression in garnet (Mg70)–orthopyroxene–sillimanite gneisses from the Rauer Group, East Antarctica. *Journal of Metamorphic Geology* **16**, 541–562.

Holland, T. J. B. & Powell, R. (1998). An internally consistent thermodynamic data set for phases of petrological interest. *Journal of Metamorphic Geology* **16**, 309–343.

Holloway, J. R. & Blank, J. G. (1994). Application of experimental results to C–O–H species in natural melts. In: Carroll, M. R. & Holloway, J. R. (eds) *Volatiles in Magmas. Mineralogical Society of America, Reviews in Mineralogy* **30**, 187–230.

Holtz, F. & Barbey, P. (1991). Genesis of peraluminous granites II. Mineralogy and chemistry of the Tourem Complex (North Portugal). Sequential melting vs restite unmixing. *Journal of Petrology* **32**, 959–978.

Holtz, F. & Johannes, W. (1994). Maximum and minimum water contents of granitic melts: implications for chemical and physical properties of ascending magmas. *Lithos* **32**, 149–159.

Holtz, F., Behrens, H., Dingwell, D. B. & Taylor, R. B. (1992*a*). Water solubility in aluminosilicate melts of haplogranite composition at 2 kbar. *Chemical Geology* **96**, 289–302.

Holtz, F., Johannes, W. & Pichavant, M. (1992*b*). Peraluminous granites: the effect of alumina on melt composition and coexisting mineral. *Philosophical Transactions of the Royal Society of Edinburgh* **83**, 409–416.

Jochum, C., Mirwald, P. W., Maresch, W. V. & Schreyer, W. (1983). The kinetics of H_2O exchange between cordierite and fluid during retrogression. *Fortschritte der Mineralogie* **61**, 103–105.

Johannes, W. & Holtz, F. (1990). Formation and composition of H_2O-undersaturated granitic melts. In: Ashworth, J. R. & Brown, M. (eds) *High Temperature Metamorphism and Crustal Anatexis*. London: Unwin Hyman, pp. 87–104.

Johannes, W. & Holtz, F. (1996). *Petrogenesis and Experimental Petrology of Granitic Rocks*. Berlin: Springer.

Johannes, W. & Schreyer, W. (1981). Experimental introduction of CO_2 and H_2O into Mg-cordierite. *American Journal of Science* **281**, 299–317.

Knop, E., Scheilk, M. & Mirwald, P. W. (1998). Incorporation of sodium into magnesium cordierite below and above the solidus. *Abstract Supplement 1, Terra Nova* **10**, 30–31.

Kurepin, V. A. (1984). H_2O and CO_2 contents of cordierite as an indicator of thermodynamical conditions of formation. *Geokhimiya* **8**, 1125–1134.

Le Breton, N. (1989). Infrared investigations of CO_2-bearing cordierites: some implications for the study of metapelitic granulites. *Contributions to Mineralogy and Petrology* **103**, 387–396.

Le Breton, N. & Thompson, A. B. (1988). Fluid-absent (dehydration) melting of biotite in metapelites in the early stages of crustal anatexis. *Contributions to Mineralogy and Petrology* **99**, 226–237.

Lepezin, G. G. & Melenevsky, V. N. (1977). On the problem of water diffusion in the cordierites. *Lithos* **10**, 49–57.

Lonker, S. W. (1981). The *P–T–X* relations of the cordierite–garnet–sillimanite–quartz equilibrium. *American Journal of Science* **281**, 1056–1090.

Martignole, J. & Sisi, J.-C. (1981). Cordierite–garnet–H_2O equilibrium: a geological thermometer, barometer and water fugacity indicator. *Contributions to Mineralogy and Petrology* **77**, 38–46.

McMillan, P. F. (1994). Water solubility and speciation models. In: Carroll, M. R. & Holloway, J. R. (eds) *Volatiles in Magmas. Mineralogical Society of America, Reviews in Mineralogy* **30**, 131–156.

McMillan, P. F. & Holloway, J. R. (1987). Water solubility in aluminosilicate melts. *Contributions to Mineralogy and Petrology* **97**, 320–332.

Mirwald, P. W. (1986). Ist Cordierite ein Geothermometer? *Fortschritte der Mineralogie* **64**, 119.

Mirwald, P. W. & Schreyer, W. (1977). Die stabile und metastabile Abbaureaktion von Mg-cordierit in Talk, Disthen und Quartz und ihre Abhangigkeit vom Gleichgewichts-wassergehalt des Cordierits. *Fortschritte der Mineralogie* **55**, 95–97.

Mirwald, P. W., Maresch, W. V. & Schreyer, W. (1979). Der Wassergehalt von Mg-cordierit zwischen 500° und 800°C sowie 0·5 und 11 kbar. *Fortschritte der Mineralogie* **57**, 101–102.

Mirwald, P. W., Jochum, C. & Maresch, W. V. (1986). Rate studies on hydration and dehydration of synthetic Mg-cordierite. *Materials Science Forum* **7**, 113–122.

Moore, G., Vennemann, T. & Carmichael, I. S. E. (1995). Solubility of water in magmas to 2 kbar. *Geology* **23**, 1099–1102.

Moore, G., Vennemann, T. & Carmichael, I. S. E. (1998). An empirical model for the solubility of H_2O in magmas to 3 kilobars. *American Mineralogist* **83**, 36–42.

Mukhopadhyay, B. & Holdaway, M. J. (1994). Cordierite–garnet–sillimanite–quartz equilibrium I. New experimental calibration in the system $FeO–Al_2O_3–SiO_2–H_2O$ and certain $P–T–X_{H_2O}$ relations. *Contributions to Mineralogy and Petrology* **116**, 462–472.

Newton, R. C. & Wood, B. J. (1979). Thermodynamics of water in cordierite and some petrologic consequences of cordierite as a hydrous phase. *Contributions to Mineralogy and Petrology* **68**, 391–405.

Newton, R. C., Smith, J. V. & Windley, B. F. (1980). Carbonic metamorphism, granulites, and crustal growth. *Nature* **288**, 45–49.

Papale, P. (1997). Thermodynamic modelling of the solubility of H_2O and CO_2 in silicate liquids. *Contributions to Mineralogy and Petrology* **126**, 237–251.

Patiño Douce, A. E. & Johnston, A. D. (1991). Phase equilibria and melt productivity in the pelitic system: implications for the origin of peraluminous granitoids and aluminous granulites. *Contributions to Mineralogy and Petrology* **107**, 202–218.

Pichavant, M., Holtz, F. & McMillan, P. F. (1992). Phase relations and compositional dependence of H_2O solubility in quartz–feldspar melts. *Chemical Geology* **96**, 303–319.

Puziewicz, J. & Johannes, W. (1990). Experimental study of a biotite-bearing granitic system under water-saturated and water-undersaturated conditions. *Contributions to Mineralogy and Petrology* **104**, 397–406.

Santosh, M., Harris, N. B. W., Jackson, D. H. & Mattey, D. P. (1990). Dehydration and incipient charnockite formation: a phase equilibria and fluid inclusion study from south India. *Journal of Geology* **98**, 915–926.

Schreyer, W. (1985). Experimental studies on cation substitutions and fluid incorporation in cordierite. *Bulletin de Minéralogie* **108**, 273–291.

Schreyer, W. & Yoder, H. S. (1964). The system Mg-cordierite–H_2O and related rocks. *Neues Jahrbuch für Mineralogie, Abhandlungen* **101**, 271–342.

Shmulovich, K. I. & Graham, C. M. (1996). Melting of albite and dehydration of brucite in H_2O–NaCl fluids to 9 kbars and 700–900°C: implications for partial melting and water activities during high pressure metamorphism. *Contributions to Mineralogy and Petrology* **124**, 370–382.

Skippen, G. B. & Gunter, A. E. (1996). The thermodynamic properties of H_2O in magnesian and iron cordierite. *Contributions to Mineralogy and Petrology* **124**, 82–89.

Smith, C. H. (1996). $H_2O–CO_2$ contents of cordierite in migmatites of the Fosdick Mountains, Marie Byrd Land. *Terra Antarctica* **3**, 11–22.

Stevens, G. & Clemens, J. D. (1993). Fluid-absent melting and the roles of fluids in the lithosphere: a slanted summary? *Chemical Geology* **108**, 1–17.

Stevens, G., Clemens, J. D. & Droop, G. T. R. (1995). Hydrous cordierite in granulites and crustal magma production. *Geology* **23**, 925–928.

Stolper, E. M. (1982). The speciation of water in silicate melts. *Geochimica et Cosmochimica Acta* **46**, 2609–2620.

Thompson, P., Harley, S. L. & Carrington, D. P. (2001) Sodium and potassium in cordierite—a potential thermometer for melts? *European Journal of Mineralogy*, in press.

Vernon, R. H. & Collins, W. J. (1988). Igneous microstructures in migmatites. *Geology* **16**, 1126–1129.

Vernon, R. H., Clarke, G. L. & Collins, W. J. (1990). Local, mid-crustal granulite-facies metamorphism and melting: an example in the Mount Stafford area, Central Australia. In: Ashworth, J. R. & Brown, M. (eds) *High-temperature Metamorphism and Crustal Anatexis*. London: Unwin Hyman, pp. 272–319.

Vielzeuf, D. & Clemens, J. D. (1992). The fluid-absent melting of phlogopite + quartz: experiments and models. *American Mineralogist* **77**, 1206–1222.

Vielzeuf, D. & Holloway, J. R. (1988). Experimental determination of the fluid-absent melting relations in the pelitic system. Consequences for crustal differentiation. *Contributions to Mineralogy and Petrology* **98**, 257–276.

Vry, J. K., Brown, P. E. & Valley, J. W. (1990). Cordierite volatile content and the role of CO_2 in high-grade metamorphism. *American Mineralogist* **75**, 71–88.

Waters, D. J. (1988). Partial melting and the formation of granulite facies assemblages in Namaqualand, South Africa. *Journal of Metamorphic Geology* **6**, 387–404.

Waters, D. J. & Whales, D. (1984). Dehydration melting and the granulite transition in metapelites from southern Namaqualand, S. Africa. *Contributions to Mineralogy and Petrology* **88**, 269–275.

White, A. J. R. & Chappell, B. W. (1988). Some supracrustal (S-type) granites of the Lachlan fold belt. *Philosophical Transactions of the Royal Society of Edinburgh* **79**, 169–181.

Winkler, B., Milman, V. & Payne, M. C. (1994). Orientation, location, and total energy of hydration of channel H_2O in cordierite investigated by *ab-initio* total energy calculations. *American Mineralogist* **79**, 200–204.

Young, E. D., Anderson, J. L., Clarke, H. S. & Thomas, W. M. (1989). Petrology of biotite–cordierite–garnet gneiss of the McCullough Range, Nevada I. Evidence for Proterozoic low-pressure fluid-absent granulite-grade metamorphism in the southern Cordillera. *Journal of Petrology* **30**, 39–60.

Zimmermann, J.-L. (1981). The liberation of H_2O, CO_2 and hydrocarbons from cordierites: kinetics, structural sites and petrogenetic implications. *Bulletin de Minéralogie* **104**, 325–338.